WETTING AND ADHESION IN ALUMINA-ALUMINUM METAL-CERAMIC INTERFACES

A Thesis

by

AHMET TIGLI

Submitted to the Office of Graduate and Professional Studies of
Texas A&M University
in partial fulfillment of the requirements for the degree of

MASTER OF SCIENCE

Chair of Committee,	Tahir Cagin
Committee Members,	Ankit Srivastava
	Zhengdong Cheng
Head of Department,	Ibrahim Karaman

May 2017

Major Subject: Materials Science and Engineering

ABSTRACT

In this work, we investigate the thermal and mechanical properties of aluminum metal and alumina (α- Al_2O_3) ceramics by performing molecular dynamic simulation (MD) using two versions of reactive force fields (ReaxFF) for Al and Al_2O_3. We also use embedded atom model (EAM) potentials for the aluminum metal simulations. The MD simulations for thermal and mechanical properties are performed for different temperatures ranging from 0 to 1400 K and pressures ranging from 0 to 8 GPa.
We also investigate the surface formation energy of solid aluminum and alumina for different temperatures. The surface formation MD simulations serve two purposes: first, to obtain the surface formation energies of aluminum and alumina using the EAM, ReaxFF potentials at different temperatures; and second, to acquire the relaxed alumina surfaces at the temperatures 700 to 1400 K in order to use the final atomic configurations of the wetting simulations as the initial structure of surfaces of alumina substrate.

The main result of this work is the investigation of the wetting and interface chemistry of molten aluminum droplets of the α-Alumina (0001) surface through MD simulations by employing the ReaxFF potentials. Wetting and interface chemistry are studied for different temperatures from 700 to 1400 K for four different droplet sizes: 16, 24, 32 and 40 Å diameters. Chemical reactions are observed at all temperatures and sizes in addition to diffusion between droplet and sphere atoms into each other during the wetting process. To define the level of wetting, we characterized contact angles of aluminum droplets on alumina substrates for all temperatures and sizes. We quantified the size and temperatures dependence of contact angle. Chemical reactions might be

more effective for the small droplets 16 and 24 Å vs the bigger droplets 32, 40 Å due to the surface volume ratio of droplets.

ACKNOWLEDGEMENTS

I would like to thanks my advisor, Dr. Tahir Cagin for support and opportunity to work on his research group and his patience and support during my thesis work. I also would like to thanks Dr. Ankit Srivastava, and Dr. Zhengdong Cheng for their time, patience, kindness as a my committee members.

I would like to acknowledge and thank for the generous financial support of the Ministry of Education of the Republic of Turkey.

Special thanks to my group fellows for their helps. Especially I would like to thanks Dr. Sevil Sarikurt, Karthik Sridhara for their help, and Ugur Aslan, Burak Ayyildiz for their supports.

Last but not least, I would like to thanks to my family, Metin Calti, Nedim Calti and Nermin Can for their encouragement, support, love and understanding.

CONTRIBUTORS AND FUNDING SOURCES

Contributors

This work was supervised by a thesis committee consisting of Professor Tahir Cagin and Ankit Srivastava of the Department of Material Science and Engineering and Professor Zhengdong Cheng of the Department of Chemical Engineering.

All work for the thesis was completed independently by the student.

Funding Sources

Graduate study was supported by a scholarship from Ministry of Education of the Republic of Turkey.

TABLE OF CONTENTS

Page

LIST OF FIGURES

Page

LIST OF TABLES

Page

1. INTRODUCTION

1.1. Background and Motivation

Composites are commonly categorized into following three classes: metal-ceramic, metal-polymer, and polymer-ceramic composites. There is strong demand from the aerospace, construction, power and transport industries [1, 2] for high performance composites because of the unique properties of composites such as high strength to weight ratio, abrasion and impact resistance and high ductility and strength [3]. In particular, metal-ceramic composites are used extensively by mechanical, oil & gas and aerospace industries [4]. The critical nature and the success of metal-ceramic composites reside at the metal-ceramic interface [5]. Therefore, the thesis is focused on metal-ceramic interfaces where the metal chosen is aluminum and the ceramic chosen is alumina.

The Al-Al_2O_3 interface is of great interest because of its high temperature creep resistance, higher fatigue strength [6], higher wear and corrosion resistance [7, 8]. Despite their interesting mechanical and physical properties, there are many issues that are yet to be addressed experimentally and theoretically. Some of the issues that are pending investigation include wetting, adhesion, kinetic and dynamic friction, and solid-liquid thermal transport. Elucidating the wetting phenomena under different environmental, thermal and mechanical conditions is very important for practical applications such as development of new metal-ceramic composite, casting smelting process, wear - corrosion protection, coatings and microelectronics technologies.

With the advances in computing technology and computational methods, computational modeling serves as a potential useful and efficient tool. Hence, we will employ computational modeling in our investigation of wetting and adhesion issues at the metal-metal oxide interfaces. Computational modeling offers a variety of tools pertinent to our investigation: in particular, the tools based on quantum level ab initio methods and molecular dynamics (MD) utilizing classical interaction potentials. Molecular dynamics with a reliable interaction potential enables us to query the state of the system and relate that to the properties of the studied system. In this study, MD is employed to assess the atomistic level interactions, underlying physical and chemical cause of the wetting and adhesion and the connections between them. In order to meet the goal of this study (to understand solid/solid and liquid/solid Al-Al_2O_3 interfaces, the wetting and adhesion phenomena at atomistic level) we specifically choose to employ reactive force fields (ReaxFF) for Al/Al_2O_3 in our MD simulations. In particular, we will investigate influence of temperature, time, size of droplet on wetting and adhesion properties of Al-Al_2O_3 interface. Since its introduction the Reactive Force Fields (ReaxFF) is becoming very critical for studying areas such as combustion, fuel cell and catalysis through MD simulations where chemical reactions play central role. Reactive force fields are capable of representing chemical reactions at the classical level by appropriate functional forms for the interaction potentials and for which the associated parameters are determined through extensive quantum mechanical/chemical methods [9].

Al-Al_2O_3 interfaces have non-wetting to wetting transition temperature from around 1150 K [10] to 1000 K [11]. The reason for different transition temperatures might be oxidation or impurities of molten aluminum metal or local structural and chemical changes at crystal planes at the alumina surface. In molecular modeling, one can create totally pure molten aluminum and crystalline alumina with oxygen and impurity free environment. Therefore, it may help better understanding of wetting of Al/α-Al_2O_3 system. MD simulations are and will be performed at different temperatures with different size of metal droplets without the environmental oxygen effects. Simulations are performed at constant pressure, temperature and number of atoms (NPT) conditions at each temperature as we investigate the Al-Al_2O_3 metal-ceramic interface.

In our study, we melt aluminum metal using NPT MD ensembles, to create the droplet we cut a molten aluminum sphere from the resulting structure at the end of this simulation. We create different size of surface/substrates from the super cells obtained from single crystal alumina (Al_2O_3) simulations. The molten aluminum sphere was put on the Al_2O_3 substrates and simulations are performed at different temperatures to observe evolution of the wetting phenomena and from equilibrium data with which we compute the contact angles as a function of thermodynamic conditions at a particular temperature. Using the trajectories, we also investigate the structure and chemical details of Al/α-Al_2O_3 interface.

1.2. Literature Review

Aluminum (Al) and alumina (Al_2O_3) are two of the most widely used materials worldwide due to variety of technological applications. Therefore, physical, chemical, electrical properties and processing methods of these two materials are heavily studied due to their scientific and technological significance. In addition, alumina - aluminum interactions are important for improvement of performance of Al/Al_2O_3 composites. Hence these systems have attracted attention of both experimentalists and computational groups[12, 13]. These groups investigated wide variety of mechanical, thermal properties, and they also investigated the production methods. In this work, we will focus on molecular dynamic investigation of wetting properties of aluminum liquid metal on Al_2O_3 ceramic. To set up the state of the understanding below we provide a brief experimental literature review of Al/Al_2O_3 system followed by a review of theoretical and modeling studies.

1.2.1. Review of experimental studies

Describing the wettability of $Al/\alpha\text{-}Al_2O_3$ system is significant for application such as casting and smelting of aluminum. Wettability of liquid-solid system can be described by measuring the contact angle of liquid droplet on solid surface at various temperatures. Contact angle of system can be measured with experimental methods. A common

method is sessile droplet experiment at which contact angle measured via microscope or camera.

Some of the experimental wettability results for Al liquid on solid Al_2O_3 ceramic surface are summarized in Table 1. Contact angle of Al/α-Al_2O_3 system has tendency to decrease with the increase at the temperature increased. However, some of the experimental data show scattering on temperature dependence of contact angle dependence [11, 14]. For example, Klinter et al. report a scatter ranging from 93º to 94º for contact angle while temperature is increased from 700 to 730 ºC (see Table 1) [11]. Furthermore, measurements of contact angle show a significant level of spread even for the same temperature at different studies. For example, contact angle is varied from 90±2º at 700 º C to 158º at 670 º C at two different studies Wang and Wu[15] , and Nicholas et al. [16], respectively. Purity level of materials, crystal structure, surface orientation of specimens and non-uniform experimental conditions such as vacuum level, furnace environment, oxygen level at experiment may cause significant change at the contact angle of Al/Al_2O_3 interfaces

Table 1: Experimental contact angle of aluminum droplet on alumina substrate

Ref.	Atmosphere	Aluminum and Alumina (substrate)	T (˚C)	Contact angle (˚)	Remark
[11]	1 bar argon, Vacuum < 10^{-9}	99.99 % aluminum 99.7% pure alumina α plane (1120) sapphire	670 700 730 750 800 670 700 730 750 800	115 93 94 87 88 122 92 84 86 83	Injection methods Multiple furnace tube
[15]	Vacuum >10^{-9} oxygen partial pressure 10^{-49}	AL sapphire	700	90±2	Injection methods
[14]	10^{-8} bar vacuum, 1 bar argon, O_2 partial pressure 10^{-21}	99.7 pure alumina 99.999 aluminum	1000 1100 1200 1300 1400	70 63 53 50inc55 Rapid evaporation	Contact heating sessile droplet methods The measurement done depend on temperature and time.
[10]	2*10^{-8} vacuum	99.9999 aluminum 99.9 pure alumina	680 750 850 950 1050	126 121 96 79 74	Sessile drop method
[17]	1 bar argon	99.99 aluminum 99.99 pure alumina (sapphire)	750 800 850 900 950 1000 1050 1100	136 127 118 110 100 95 90 88	Contact heating sessile drop method Semi cylindrical refractory steel segments
[18]	Vacuum 5*10^{-9}	99.99 aluminum 99.99 pure α-Al_2O_3 single crystal	700 800 900 1000 1100	127 130 120 110 97	Sessile drop method Continuous oxidations

Table 1 Continued

Ref.	Atmosphere	Aluminum and Alumina (substrate)	T (˚C)	Contact angle (˚)	Remark
[19]	Vacuum $6.6*10^{-2}$	Loose Al_2O_3 Annealed loose Al_2O_3 Commercial Al_2O_3	950 1250 950 1250 950 1250	121±2 125±2 124±2 122±2 126±3 54±3	Sessile drop test SEM, EDS and TEM

1.2.2. Review of computational studies

Wetting and interfacial properties, and chemical reactions of Al/Al_2O_3 interfaces are measured and investigated via experimental methods. However, the aluminum and alumina interfaces may still need further investigation. Since the experimental methods have difficulty and limitations to show atomistic correlations at liquid-solid interfaces; computational methods such as molecular dynamics (MD), density functional theory (DFT) can be used for a deeper understanding of microscopic and atomistic level of wetting phenomena at the different temperatures. However, the quantum mechanical calculations such as DFT are very computationally expensive to perform for such large size systems. Therefore, molecular dynamic methods can be a good option to investigate the wetting of Al/Al_2O_3 system. Consequently, MD calculations are frequently performed to examine wetting properties, adhesion and surface formation energy, and oxidation of metals for the metal-ceramic system [13, 20-22].

Recently several molecular dynamic simulations have been performed to investigate microscopic (atomistic) level interactions for metal-ceramic interfaces. As an example,

Cagin and coworkers investigated elastic constants, adhesion, and surface formation energies of solid Al and Al_2O_3[13]. They also investigated the transition from non-wetting to wetting of liquid Al on Al_2O_3. Pilania and Thijsse et al. have also investigated the coherent and semi-coherent Al/Al_2O_3 interfaces for oxygen and aluminum rich interfaces at different temperatures [23]. They reported observing three sets of dislocations and regions similar to stacking-faults at the interfaces.

Zhang et al. have also investigated velocity dependency of kinetic friction of solid/solid interface for Al/Al and Al_2O_3/Al_2O_3[24]. They also studied adhesion and static friction for commensurate and incommensurate alumina/alumina surface, and rough and smooth Al/Al surface. Aral et al studied the oxidation of flat aluminum dependency on oxygen pressure and time [23]. They observed temperature increase at the O/Al interfaces, and they report that oxidation thickness of flat Al increases with time. Aral also investigated the wetting of Al droplet on the Al_2O_3 as a function of temperature[1].

2. COMPUTATIONAL METHODS

Molecular level computational methods (in particular molecular dynamics) are very important to understand how the material behavior is affected by temperature, pressure, number of molecules, concentration, time and position of molecules. These methods also can be utilized to determine the stable crystal structure of materials, predict some properties such as mechanical, electronic, thermal, magnetic and chemical properties of materials.

Macroscopic properties of material are a result of the microscopic level interactions that can be defined through associated microscopic level expressions at the atomistic level. Atomistic level molecular dynamics studies are commonly performed from picosecond to nanosecond time scales with femtoseconds resolution. While macroscopic behavior and properties are commonly investigated via experimental techniques, addressing the atomistic behavior of materials is much more challenging using experimental techniques. This is due to the "black box" nature of performing experiments at the atomistic level where even small time and temperature variations may affect the overall outcome. Therefore, theoretical and computational methods are complimentary to experimental techniques. Furthermore, computational methods have some advantages over experimental techniques: in many cases the computational methods may have lower cost, less labor-intensive, may have shorter time requirement to study material properties. Finally, the atomic simulations also enhance knowledge by providing data on the atomic-level behavior of the material.

Briefly stating, there are two primary methods pertinent to our work: 1) Quantum mechanics plays a critical role in atomistic level simulations and incorporating quantum mechanical principles, such as charge transfer, improve the accuracy of the simulated results. However, this also makes for a computationally intensive simulation. 2) Interaction potential-based methods can be used to solve systems with large number of atoms. Among these method, molecular dynamics is the one of the widest used computational method, which is extensively utilized to investigate physical and chemical behavior of materials from a few atoms to millions of atoms.

2.1. Introduction to Molecular Dynamic

Molecular dynamics (MD) is a method models material systems on the basis of physical rules such as equations of motions, thermodynamic ensembles (microcanonical, canonical etc). Therefore, we need to define a material system that could mimic the bulk of single metal or single crystal ceramic or metal drop and ceramic interface structure.

Models for MD simulations can be expressed in a few stages. First of all, one creates the initial structure of system such as the type of atoms, their positions, within a volumetric domain and appropriate boundary conditions. Second, a force law describing the interaction between these atoms through an interaction potential form and with the associated interaction potential parameters. Third, specifying the environmental or thermodynamic conditions represented by appropriate statistical thermodynamic ensemble such as NVT or NPT. To initiate the MD simulation one provides a velocity distribution for the atoms of the system to represent the thermal state of the system.

Thus, upon these definition, one performs the molecular dynamic simulation for the system via solving the equations of motion. Lastly, evaluating the microscopic expressions for thermodynamic variables for each time step of simulations, through averaging them in time one calculates the corresponding macroscopic measurable properties. Furthermore, through the analysis of the trajectories generated in simulations we may obtain necessary structural properties trough averaging.

The microstate of the system is in an MD calculations simulation at each time step is given by the positions and momenta (velocities) of N atoms. Using the position of these atoms, one can evaluate the interaction forces on each of the atoms. For instance, the distance between each atom pair can be obtained using $r_i - r_j = r_{ij}$ where r_i, r_j are the coordinates of atoms i and j, at time t; through which one can calculate the pairwise forces.

Defining the interactive potential, which is used to find the force between particles, is very crucial for MD. Because MD calculations solve the equations of motion for the system which we defined previously include N atoms. Therefore, equations of motion can be described as in eq. (1)

$$F_i = m_i a_i \tag{1}$$

where F, m, a are force, mass and acceleration of the atom i, respectively. Then the equations of motion are solved iteratively for each time step for updating positions and velocities for the next iteration. As the interactions between particles can be recalculated

for the next iteration this cycle generated the trajectory (r, and p) as a function of changing in position. The force on each atom of the system can be defined from the partial derivative of total energy as in eq. (2).

$$F = -\frac{\partial E}{\partial r} \tag{2}$$

Most of the modeling method and system start with describing the initial conditions such as crystal structure, material and thermodynamic conditions such as statistical thermodynamic ensembles which are discussed in the next section. To complete the model system to be simulated one needs to provide the manner with which the particles interact with each other, the interaction potentials, both functional forms and appropriate parameters for the specific system, which is used in evaluating energy, forces and other relevant microscopic properties as a function of positions of the atoms (through the positions one may define distances, angles, etc, which may enter into functional forms of the interaction potentials). We will discuss the interaction potentials in more detail below in section (2.6).

2.2. MD Simulations and Associated Statistical Thermodynamic Ensembles

To develop the accurate material models, environmental conditions of the system should be defined. MD employs classical dynamics to a collection of particles, the properties of the system is measured/determined through statistical mechanics via using equivalence of time averages to ensemble averaging. Hence microscopic properties are

averaged over time for each configuration and momenta of N-body system for each time step. The measurable macroscopic properties are these time averaged properties and they are produced through trajectories generated under predefined specific thermodynamic conditions, hence one employs different statistical thermodynamic ensembles in various forms of MD simulations. MD simulation can be performed at different thermodynamic and mechanical conditions such as constant number of particles, constant temperature, constant volume, constant pressure or constant energy, etc. These conditions are dictated by the thermodynamics. To list the most widely encountered conditions: microcanonical NVE ensemble [constant energy and constant volume (isochoric)], canonical NVT ensemble [constant temperature (isothermal), isochoric] or isobaric ensembles, NPT and NPH (isothermal-isobaric, isoenthalpic-isobaric). In all these the number of particles kept constant. The methods beyond microcanonical (NVE) ensemble, i.e. to generate the trajectories in other ensembles for MD simulation are developed early 80's [25-30]. The simulations under variable particle conditions were also developed in early 90's [31, 32].

In NVE (microcanonical) system, the system is adiabatically isolated where there is no transfer or exchange of particle. Therefore, the number of particle will stay constant. Energy of the system is also constant, meaning that there is only internal energy of system. Therefore, there is no energy exchange with the surrounding. In addition, the volume of the system is also constant. NVE ensemble can be used to calculate stable lattice parameter of crystal system by fitting energy vs distance curve.

Another very useful ensemble is the NVT (canonical ensemble) for MD methods. In this ensemble, the number of particles, the volume and the temperature of system are

kept constant. On the other hand, energy of the system can change depending on the configuration of atoms and temperature of the system. This ensemble can be used to perform wetting calculations.

NPT (isothermal-isobaric) ensemble is also significant for MD calculation. The volume of this model can change but the number of particles, the temperature and pressure of system are constant. Due to this there is constant T and P bath surrounding the system. NPT system is very useful to study the thermal and mechanical properties such as specific heat and bulk moduli of material systems.

2.3. Verlet Algorithm

In MD calculations, one of the most important steps is the evolution of the positions and velocities of atoms as a function of time in the system. To determine the evolution of the configurations of atoms we need to have an algorithm to solve the equations of motion. The algorithm should be simple, efficient, stable, preferably time reversible, and accurate for equations of motions. We have used Verlet algorithm in our simulations.

$$r(t+dt) = r(t) + v(t)dt + \frac{1}{2}a(t)dt^2 + b(t)dt^3 + \cdots \quad (3)$$

$$r(t-dt) = r(t) - v(t)dt + \frac{1}{2}a(t)dt^2 + b(t)dt^3 + \cdots \quad (4)$$

where dt is the time step and it should be small enough to estimate the results accurate and stable. In addition, it should be time reversible because equation of motion is time reversible.

$$r(t) = 2r(t) - r(t - dt) + a(t)dt^2 + 0dt^3 + \cdots \quad (5)$$

Subtracting equation 3 from 4, we get

$$v(t) = \frac{r(t + dt) - r(t - dt)}{2dt} \quad (6)$$

If we know the vibrational modes of the system and take a time step around 2 or 5% of that period associated with the fastest mode, for the range for time step is reasonable to solve accurately the equations of motion. A larger time step may induce larger oscillations in the total "conserved" energy (if the simulations done under the microcanonical ensemble conditions) when using the Verlet algorithm. Verlet algorithm as a time reversible algorithm as opposed to the predictor corrector algorithms avoids drift in 'conserved' energy.

2.4. Thermodynamic Properties

When MD simulations are completed, the raw data will be in the form of instantaneous temperature, pressure, internal energy, density, positions, velocities of the particles. Average values of the instantaneous quantities related to thermodynamically measurable macroscopic properties, such as Temperature, Pressure, Density, etc. These

average values further can be used to describe some thermal and mechanical response functions such as thermal expansion coefficient, specific heat capacity, bulk modulus etc. Melting point of materials can also be found from MD simulations as shown in the graph. Thermodynamic definition of physical (thermal) properties can be used to calculate the C_p specific heat capacity at constant pressure, bulk modulus (β), compressibility factor (χ), the volumetric thermal expansion coefficient (α_p).

Thermal expansion coefficient can be defined as change of volume as a function of temperature at constant pressure. The slope of Volume – temperature curve to initial volume is definition of the volumetric thermal expansion coefficient see eq. (7). Sharp change at slope is the indication of a phase transformation of material (in this case solid-liquid phase transition) as shown in Figure 1. Melting of solid is a phase transformation from solid structure to liquid. Therefore, abrupt changes of the slope of temperature vs volume curve at near experimental melting of material can be called as melting point for materials at that specific simulations see graph.

$$\alpha_p = \frac{1}{V}\left(\frac{dV}{dT}\right)_P \tag{7}$$

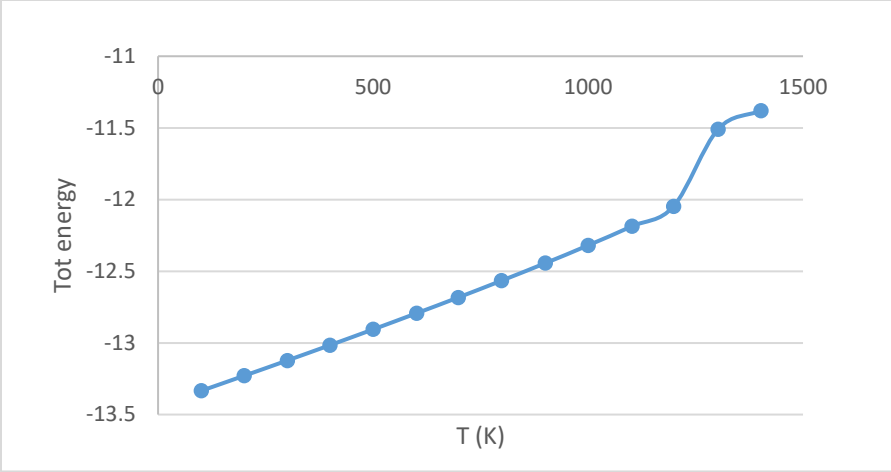

Figure 1: The temperature vs total energy graph of aluminum metal

Bulk modulus or (its inverse, compressibility) can also be defined by eq. (8) through the thermodynamic relationships of pressure vs. volume curves under constant temperature (isotherms)

$$\beta = -V\left(\frac{dP}{dV}\right)_T \quad \chi = -\frac{1}{V}\left(\frac{dV}{dP}\right)_T \tag{8}$$

2.5. Distribution Functions (One Body and Radial Pair Distributions)

MD simulations performed in a chosen thermodynamic state, (at a given temperature and/or pressure) provides evolution of the positions and velocities of the particles as a function of time through solving the equations of motion. The coordinates and velocities at a given time provide a data for the microstate of the system at that particular time. The temporal-time ordered-series of positions and momenta of particles constitute a collection of microstates in the phase space of the system. Due to temporal order in the

set of positions and momenta of particles one usually call this data as the trajectory of the system under this thermodynamic conditions, any given property of the system may be evaluated from this trajectory through averaging over long enough time using the appropriate functional form of the microscopic description of property (expressed as a function of positions and momenta). Structural properties may be considered as one of these properties. Among the structural properties of the systems, pair correlation function (or radial distribution function) is the most common one used by the practitioners of the field. Given the problem we are aiming at solving for instance we may define some specific structure related properties, such as one body distribution at the interface in the case of wetting, and evolution of the chemistry at the interface, etc. To obtain these we use the time dependent configurations, average over time and correlate over a spatial distance.

2.5.1. Radial pair distribution function: g(r)

Pair correlation function, also referred as radial distribution function (RDF), is used to describe the distribution of particles around one particle. The pair correlation function (g(r)) provides information on the structural organization of atoms constituting the system, (Solid/liquid, crystal / amorphous, ordered/disordered etc.). The pair correlation function is defined by the equation

$$g(r) = \rho^{-2} \langle \sum_{i} \sum_{i \neq j} \delta(r_i)\, \delta(r_j - r) \rangle \tag{9}$$

$$\rho^{-2} = \frac{V^2}{N^2} \tag{10}$$

where ρ is the number density of atoms (N/V), δ represents the Dirac delta function, expression above signifies a pairwise sum, by selecting atom i as the atom around which the organization of atoms j, summing over all i's and j's one collects the instantaneous state of the radial correlation by recording this information at each time step, if the correlations are averaged over time this yields the structure of the system, at the simulated temperature and pressure or volume.

The significance of radial distribution function is not by choice as it is related to the diffraction and light scattering experiments. One can relate g (r) to S(k) the structure factor that is measured directly from various forms of scattering experiments such as x-ray diffraction. Pair correlation function is real space representation of S (k) (the structure factor obtained through experiments) or vice a versa.

2.6. Interatomic Potentials

Molecular dynamics solves the equations of motions for a many body systems. In these equations, force on any particle is the result of interactions of between particles given by the interatomic potentials. Therefore, describing and choosing the interatomic potential for MD simulation is the most critical steps as they have a strong correlation with the calculated physical properties and the accuracy of the results. Over the years, wide range of interatomic potentials that are developed and used in molecular dynamic simulations. The forms of the interaction potentials are dictated by the physics and

chemistry of the systems under consideration. Most common form of interaction potentials refer to two-body interactions between atoms of the systems. Among these the description of van der Waals forces in inert gases is based on induced dipole induced dipole interactions –attractive part. Ionic systems naturally due to charges have electrostatic interactions, which is described through Coulomb law. Description of metals require going beyond two-body interactions due to conduction electron mediated many body interactions, which led various forms of many body formulations for metals. The treatment of organic systems where covalent interactions are critical, involve two body bond-stretch, three body angle bending, four body bond rotation (torsion or dihedral terms) in addition to two body van der waals and electrostatic forces. The forms and parameters for main group elements are developed an implemented by different research groups led to force fields such as AMBER, CHARMM, DREIDING force fields. Almost all these force fields fall into a category which we call non-reactive interaction force fields. However, over the past three decades, the need for studying systems with chemical reactions arouse. This in turn triggered the development of functional forms and parameterization of interaction potentials with capability of realizing chemical reactions and charge transfer at the classical level. Earlier forms of such force fields were bond order dependent force field for C, H, Si, O, etc. More recently, around a decade or so ago, a more general form embodied this capability were proposed and developed by van duin et al. These force fields were originally proposed for hydrocarbons and main group elements, is called ReaxFF. ReaxFF has since been extended to many other elements and employed in many challenging problems.

Recent trend in parameterization of interaction potentials is accomplished via fitting the energy-configuration behavior of the potentials to the associated equivalent advance quantum mechanical/quantum chemical results. In refinement of parameterization empirical properties are also utilized for increasing the reliability of the simulations. In order to mimic the physical and thermal properties of bulk materials such as stiffness constant, thermal expansion coefficient, etc. This is done for non-reactive potentials as well. They are computationally cheap in simulations. However, these potentials cannot represent chemical reactions, charge transfer, oxidation of metals or non-equilibrium conditions. Consequently, non-reactive potentials cannot be employed for simulations that require charge transfer, bond formation or dissociation between atoms such as the ones we anticipate in our interface structure / chemistry in Al/Al_2O_3 and wetting of Alumina by molten aluminum.

Chemical reactions, bond formation/dissociation etc. are very important to describe certain material properties and behavior such as corrosion, oxidation, and adhesion. Even though quantum mechanical calculations can represent the reactions between atoms and electrons, it is very hard to employ quantum chemical methods to large size problems involving on the order of a few hundreds of atoms. However, large size simulations are very important to simulate size dependent properties such as wetting. Therefore, reactive potentials are significant for realistic molecular dynamic simulations to represent chemical reactions such as oxidation of metals [33].

Reactive potentials account for the bond order, bond breaking and formation in molecular systems. Therefore, they can be used for molecular dynamic simulations in

which chemical reactions take place. Even though reactive force field is computationally expensive compared to the conventional (non-reactive) potentials as it can be seen from the functional forms described in the next section, reactive potentials are developed and heavily used in many MD simulations over the last decade.

2.7. ReaxFF (Reactive Force Fields)

Classical interatomic potentials capable of describing structure and properties with correct chemistry is critical in a molecular dynamics investigation of interfacial phenomena such as wetting and adhesion phenomena of Al/Al_2O_3 system. ReaxFF describes accurately the physical and mechanical properties of bulk aluminum, alumina and Al/Al_2O_3 interfaces. In Al/Al_2O_3 system such as wetting simulations, ReaxFF will facilitate proper representation of bond formation, dissociation and charge transfer between atoms.

ReaxFF combines classical pairwise energy terms such as van der waals and electrostatic interactions with chemical bonding energy terms – specifically parameterized from the data obtained from QM computations. Currently, ReaxFF is employed for a wide range of MD simulations from hydrocarbons to metal/ceramic interfaces.

2.7.1. Time and length of ReaxFF calculations

Computational methods for material systems have time and size limitations due to computational and real time expense. A representation of this limitation is shown in

Figure 2. The time and size limitation for computational methods increases from the QM calculation through MD, MESO and FEA (finite element analysis). As an example, time and size range of MD simulations reach the restrictive limits that might be millions of atoms or hundreds of nanoseconds (ns).

MD simulations performed with ReaxFF promise similar results that are obtained from QM calculations but the simulations are made possible for larger material system sizes. The system size in simulations could be hundreds of thousands of atoms and a couple nanoseconds long. Therefore, ReaxFF is a bridge between QM and classical MD calculations.

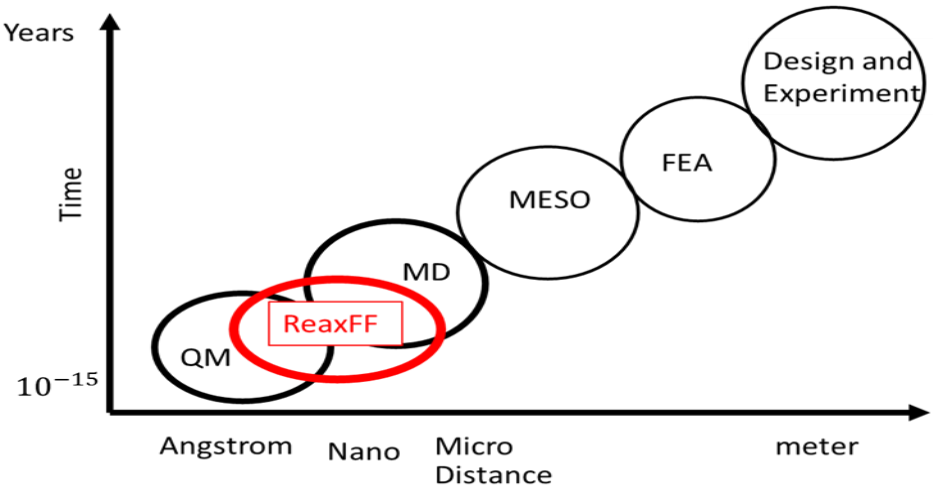

Figure 2: Comparison of computational methods for material system on time vs size.

2.7.2. Formalism of ReaxFF

Current formalism of reactive force fields (ReaxFF) has some additional terms on top of original ReaxFF [9]. Therefore, there is a small change if we compare the 2001 hydrocarbon and 2003 silica papers. Despite the small change on formalism, the main concept of ReaxFF is similar to the original form of 2001 ReaxFF such as single, double and triple bonds. Three body conjugation terms are added to include formation of oxygen lone pairs and group chemistry in 2003. Although, the ReaxFF have stable functional forms, optional terms have later been added[34].

ReaxFF potential defines the system energy combination of various energy term contributions see eq. (11). Bond order formalism in ReaxFF describes both reactive and non-reactive interactions between atoms.

$$E_{sys} = E_{bond} + E_{under} + E_{over} + E_{tors} + E_{angle} + E_{vdWaals} + E_{Coul} + E_{specific} \quad (11)$$

where E_{bond} describes the bond formation energy between atoms. $E_{vdWaals}$, E_{Coul} are dispersive and electrostatic calculation between all atoms, respectively. The torsion angle strain between four atoms and angle strain between three atoms represents associated energies E_{tors} and E_{angle}. E_{over} and E_{under} are the penalty energies that prevent over coordination and under coordination of atoms, respectively. $E_{specific}$ are specific terms such as hydrogen or oxygen binding which do not include regular ReaxFF [34].

2.7.2.1 Bond order

Formalism of ReaxFF is a combination of bond-order-dependent ($E_{bond},\ E_{under}, E_{over},\ E_{tors}\ , E_{angle}$) and independent terms ($E_{vdWaals}, E_{Coul}$). Bond-order-dependent terms, which are dependent on distance between atoms, can be calculated using empirical formulas, see equation (12).

$$BO_{ij} = BO_{ij}^{\sigma} + BO_{ij}^{\pi} + BO_{ij}^{\pi\pi} \tag{12}$$

$$= exp\left[P_{bo1}\left(\frac{r_{ij}}{r_0^{ij}}\right)^{P_{bo2}}\right] + exp\left[P_{bo3}\left(\frac{r_{ij}}{r_0^{\pi}}\right)^{P_{bo4}}\right] + exp\left[P_{bo5}\left(\frac{r_{ij}}{r_0^{\pi\pi}}\right)^{P_{bo6}}\right]$$

where the term BO_{ij}, r_{ij}, r_0^{σ}, $r_0^{\sigma\pi}$, $r_0^{\pi\pi}$ are the bond order, interatomic distance and equilibrium distances for single, double and triple bond between atoms i and j, respectively. P_{boi}, i 1 to 6 are bond order parameters of ReaxFF which are obtained from QM and experimental data. The bond order equation is continuous and inversely proportional to the distance between atoms. Therefore, ReaxFF can describe partial bonds and transition state for material simulations.

ReaxFF defines the coordination of atoms with the other atoms by employing bond-order correction scheme. Therefore, formation and dissociation of bonds are controlled using under- and over co-ordination penalty energies. Therefore, if the coordination of atom exceeds the valance electron number (allowed number of coordination), the primary bonds continue but weak bonds reduced until allowed number of bond. Thus, ReaxFF can simulate the transition states, chemical reactions.

3. THERMODYNAMIC AND MECHANICAL PROPERTIES OF Al AND Al2O3

3.1. Computational Details

In our calculations, we employed molecular dynamic methods to study mechanical and thermodynamic properties of aluminum metal and alumina (Al_2O_3) ceramic, and we used two different potential types for Al and Al_2O_3. A third type potential is also used for aluminum: embedded-atom method (EAM) [35] which is parametrized by Mishin and Farkas etc. in 1999 [36]. Two types of ReaxFF, first one developed by Q, Zhang et. al. in 2004 [13] and the second one is a re-parameterized version of ReaxFF for Al and Al_2O_3 system which is developed by S. Hong et. al. [22] (shown in Table 2). We decided to compare the two-parameterized version of ReaxFF. I call them ReaxFF (2004) and ReaxFF (2014) corresponding to the year the respective papers were published. We employed Large Scale Molecular Massively Parallel Simulator (LAMMPS) MD simulator which is developed by Sandia National Laboratories[37, 38]. These MD calculations performed at Texas A&M University, High Performance Research Computing facilities, ADA Cluster.

Table 2: Potential types used in simulations of aluminum metal, alumina ceramic and aluminum/alumina wetting

	EAM	ReaxFF (2004)	ReaxFF (2014)
Aluminum (metal)	Used	Used	Used
Alumina (ceramic)	---	Used	Used
Al/Al_2O_3 (interface)	---	---	Used

3.1.1. Comparison between ReaxFF (2004) and ReaxFF (2014)

The ReaxFF (2004) is developed and used by Zhang and Cagin et al. for wetting and adhesion simulations of Al/Al_2O_3 interfaces [13]. And they used the same potential to define kinetic friction and velocity dependency, and static friction and relationship to adhesion [24, 39]. The general expression for ReaxFF (2004) is shown at eq. The total energy term for aluminum and alumina is combination of coulombic, van der walls, bond and over-coordination terms. Coulombic intentions were calculated for all Al-Al and Al-O pairs. Electron equilibration methods used to determine the $E_{coulomb}$ (Coulombic parameters). The ReaxFF (2004) include bond stretched terms, but it does not include valance angle and torsion terms. It enables atoms to charge transfer between aluminum and oxygen atoms.

$$E_{system} = E_{Coulomb} + E_{vd\,Waals} + E_{bond} + E_{over} \tag{13}$$

The ReaxFF (2014) is used by Hong and van Duin for oxidation of aluminum nanoparticles[22]. The potential description contain and extend the ReaxFF (2004) descriptions [34]. The general expression for ReaxFF (2014) is shown at eq . the total energy term of ReaxFF (2014) is combination of two body, three body, four body and multi body terms. These are coulombic ($E_{Coulomb}$), van der Waals ($E_{vd\,Waals}$), bond energy (E_{bond}), valance angle (E_{angle}), torsion angle (E_{tors}), under and over coordination (E_{over}, E_{under}) terms. Detailed information on ReaxFF (2014) available in Hong and van Duin [22].

$$E_{system} = E_{Coulomb} + E_{vd\,Waals} + E_{bond} + E_{lp} + E_{angle} + E_{tors} + E_{over} + E_{under} \quad (14)$$

The ReaxFF (2014) and ReaxFF (2004) have the same functional form. However, the potentials have different parametrization for bond energy, and over-under coordination terms. Additionally, ReaxFF (2014) have three body and 4 body terms which are valance angle and torsion angle terms.

3.2. Crystal Structure of Al and Al_2O_3

The stable crystal structure of aluminum metal is face centered cubic (fcc), and we used this crystal structure in our calculations with the initial lattice parameter, a=4.05 Å. We created an FCC super cell consisting of 4000 atoms, and the lateral size is 40.5 Å in x, y and z directions. The super cell is used to calculate bulk properties of Al metal, such as volumetric thermal expansion coefficient, bulk modulus etc.

Alumina has several polymorphs namely corundum (α-Al_2O_3), β-Al_2O_3 and **γ**-Al_2O_3 crystal structures but α-Al_2O_3 is thermodynamically stable form of alumina. Therefore, we chose to use the α-Al_2O_3 form for our studies. Crystal structure and space group of α-Al_2O_3 are 169 or R3c with hexagonal lattice. We used 4.748 Å for a and b lattice parameters and 12.96 Å for c lattice and angles are α=**γ**=90˚ and β=120˚. To create a supercell of α-Al_2O_3, we write a script and we used the generated crystal structures for MD calculations as an initial structure of the system.

To determine bulk thermal properties such as volumetric thermal expansion and specific heat of Al and Al_2O_3, we used NPT ensemble MD. These simulations were

performed at constant pressure, 0 bar, and the temperature is increased from 0 to 1400 K in 100 K increments. We performed MD simulations consisting of three segments for every 100 K. Segment 1: heating run, 10 picosecond (ps); Segment 2: relaxation run, 4 ps and Segment 3: equilibrium run, 20 ps long simulation for data collection. The averages of temperature, pressure, volume, energy, etc. were taken from the equilibrium simulations at each temperature. For MD simulations time step is very important. We chose to use two different time steps in our simulations. In ReaxFF simulations, 0.2 fs time-step gives stable results in addition that we use 100 for temperature damping factor, but for the EAM based simulations, 1 fs time-step also gives stable results with 10 for temperature damping factor. The total thermal scanning calculations span over 170000 time-steps (34 ps) increasing temperature by 100 K for 0 K to 1400 K. Therefore, the total length of the calculation is around 500 ps and 2400 ps for ReaxFF, and EAM simulations, respectively. These simulations have also been used to determine the melting behavior of Al. We also have determined the structural properties by analyzing the trajectories for each temperature for pair distribution functions.

3.2.1. Thermal expansion coefficient

Thermal expansion coefficient can be defined as the change of volume with respect to temperature at the given constant pressure. We can calculate volumetric thermal expansion coefficients from constant pressure NPT simulations. We report the calculated thermal expansion coefficients of Al metal for three potentials and Al_2O_3 for two ReaxFF potentials below.

3.2.1.1. Al metal using EAM and ReaxFF

Aluminum heating simulations show that the ReaxFF (2004) has the same melting temperature as the ReaxFF (2014) but lower than the EAM potential. However, the EAM potential displayed a later the melting temperature compared to ReaxFF potentials. The simulations performed under the same condition and the same number of atoms which is 4000 atoms (1000 fcc unit cells). Therefore, there is no size effect comparison made on the simulation results. However, the only exception is the difference between three potentials which affect the simulation results.

We can calculate volumetric thermal expansion coefficient (α_p) by using the average temperature and volume curve of MD results shown in Figure 3. And we calculated α_p by using those curves (refer Table 3). Experimental value of volumetric thermal expansion for aluminum is 7.08×10^{-5} [40, 41].

The thermal expansion coefficient of aluminum metal calculated with the ReaxFF (2004) is larger than EAM. However, the ReaxFF (2014) calculation resulted in an even larger thermal expansion coefficient than both the ReaxFF (2004) and EAM potential. The temperatures above the melting point, the thermal expansion coefficient is even larger for ReaxFF (2014). EAM represents a closer approximation for thermal expansion coefficient of aluminum of the three potentials.

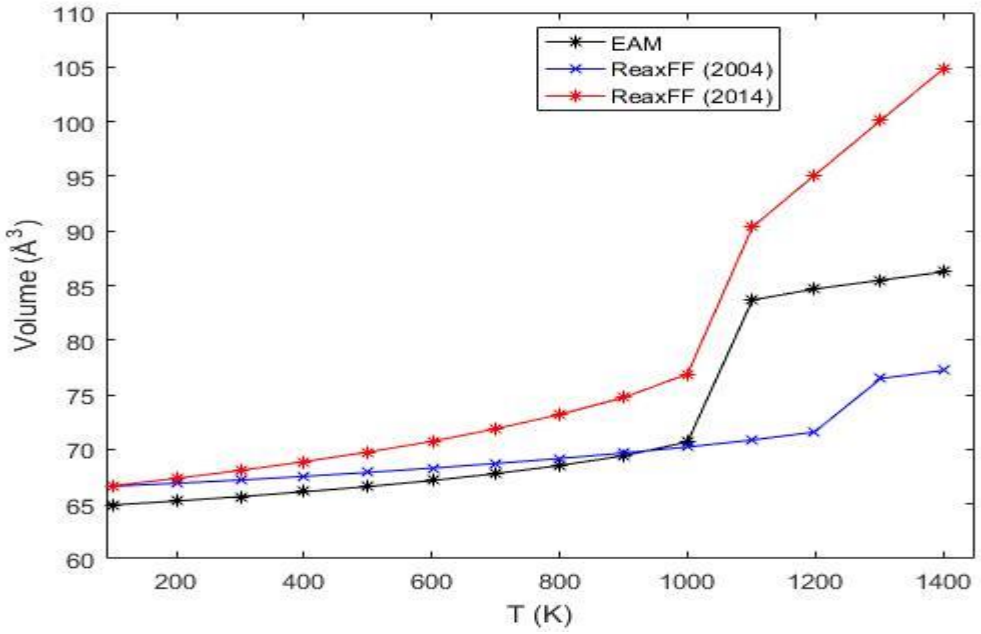

Figure 3: The temperature vs volume curves of Al metal with EAM, ReaxFF (2004) and ReaxFF (2014)

Table 3: Volumetric thermal expansion coefficient ($\boldsymbol{\alpha_p}$) of Al metal with EAM, ReaxFF (2004) and ReaxFF (2014)

	Exp.	EAM	ReaxFF (2004)	ReaxFF (2014)
Solid $\alpha_p\ (K^{-1})$	$6.9x10^{-5}$ [a]	$6.681x10^{-5}$	$9.5517 * 10^{-5}$	$16.8 * 10^{-5}$
Liquid $\alpha_p\ (K^{-1})$			$11.42 * 10^{-5}$	$130.7 * 10^{-5}$

[a] Reference [41]

3.2.1.2. Al_2O_3 with ReaxFF (2004) and ReaxFF (2014)

Volumetric thermal expansion coefficient of Al_2O_3 was also calculated from temperature vs volume curve of heating up simulations for reaxFF (2004) and (2014). Al_2O_3 ceramic heated up from 0 to 1400 K using NPT simulations. We observed abrupt changes in the temperature vs volume curve for ReaxFF (2004), but ReaxFF (2014) has

a very nice and smooth increase at volume with temperature (see Figure 4). Therefore, we chose to calculate thermal expansion for 0 to 500 K for ReaxFF (2004) (see Figure 5 refer Table 4). However, we calculated thermal expansion of Al_2O_3 from 0 to 1400 K for ReaxFF (2014) (refer Table 4). Experimental value of linear thermal expansion coefficient of alumina is 7.6×10^{-6} K^{-1} [40, 42].

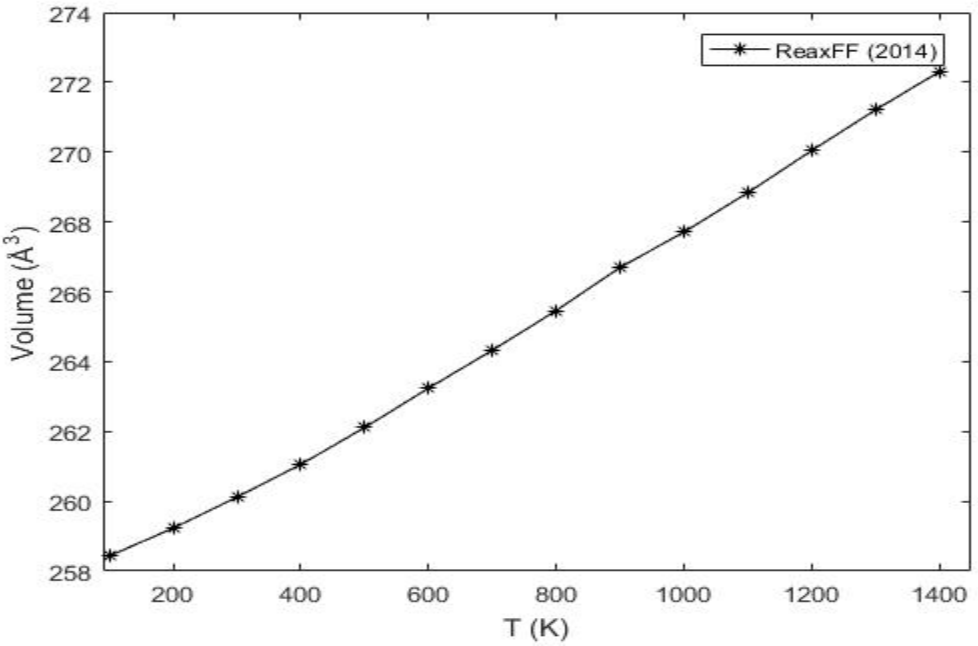

Figure 4: The temperature vs volume of alumina for heating up simulation with ReaxFF (2014)

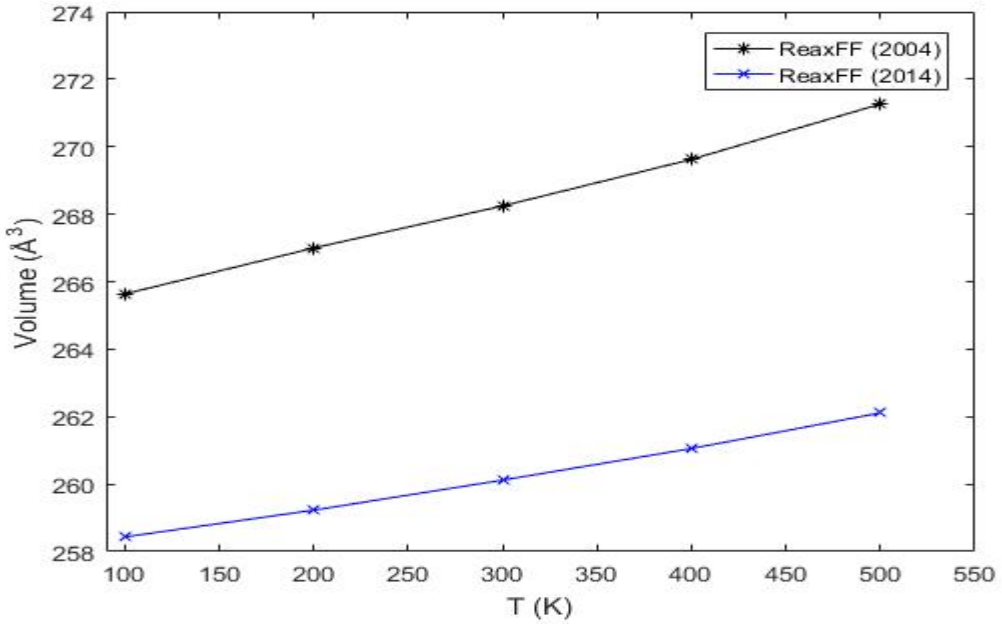

Figure 5: The temperature vs volume in alumina from heating up simulations with ReaxFF (2004) and 2014 in solid phase from 100 K to 500 K

Table 4: Volumetric thermal expansion coefficient (α_p) of Al_2O_3 from simulations with ReaxFF (2004) and ReaxFF (2014)

	Exp.	ReaxFF (2004)	ReaxFF (2014)
Solid α_p (K^{-1}) (0-500 K)	1.6*10^{-5} [a] at 300 K	$5.261 * 10^{-5}$	$3.576 * 10^{-5}$
Solid $\alpha_p(\ K^{-1})$ (0-1400 K)		--------	$4.243 * 10^{-5}$

[a] Reference [43]

3.2.2. Cooling of Al and Al_2O_3

We also cooled Al and Al_2O_3 from 1400 K, which is the maximum temperature of previous simulations, to 200 K. We performed heating (up to 1400 K) and cooling (down to 200 K) for both Al and Al_2O_3, employing the EAM and the ReaxFF potentials.

Because we want to observe the difference between the heating and cooling simulations. The main reason of the cooling simulations is to observe super heating and cooling phenomena, which is reported for Ni nanocluster by Qi and Cagin [44]. We make similar observations and they conclude that the real melting point of Al is somewhere between the melting point at heating and the solidification point of cooling.

In the cooling simulation, we used the NPT ensemble with the same time steps and temperature damping factors, with the increment of 100 K. The only difference between heating up and cooling down simulations is the 4 ps cooling down region instead of heating up region for example from 1400 to 1300 K.

3.2.2.1. Comparison of heating and cooling for aluminum

We observed that the heating and cooling curves of Al metal are not the same and as expected from simulations with periodic boundary conditions there is a significant superheating and supercooling behavior (shown in Figure 6 and Figure 7).

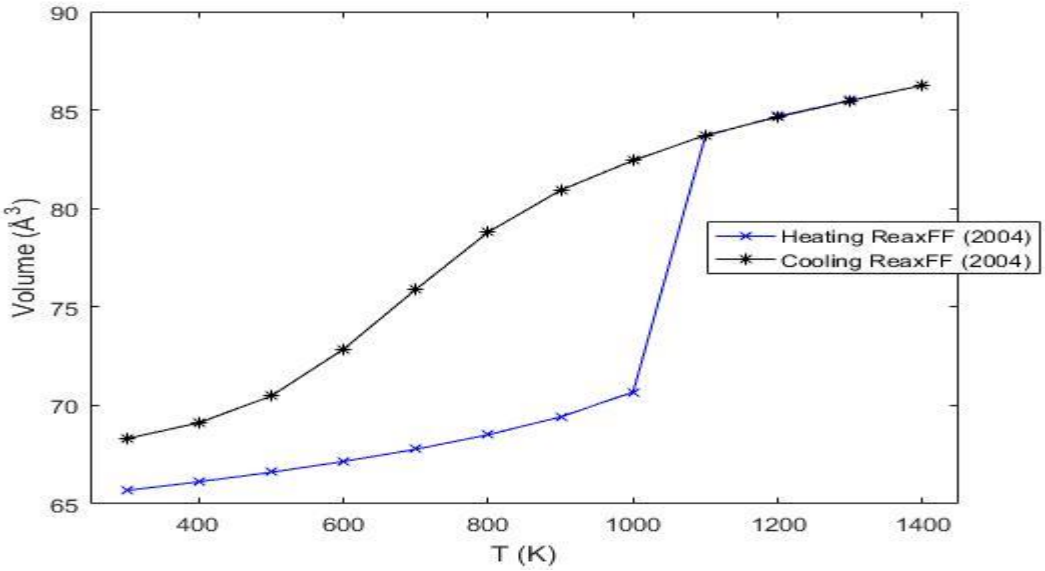

Figure 6: The temperature vs volume curves of heating and cooling of ReaxFF (2004)

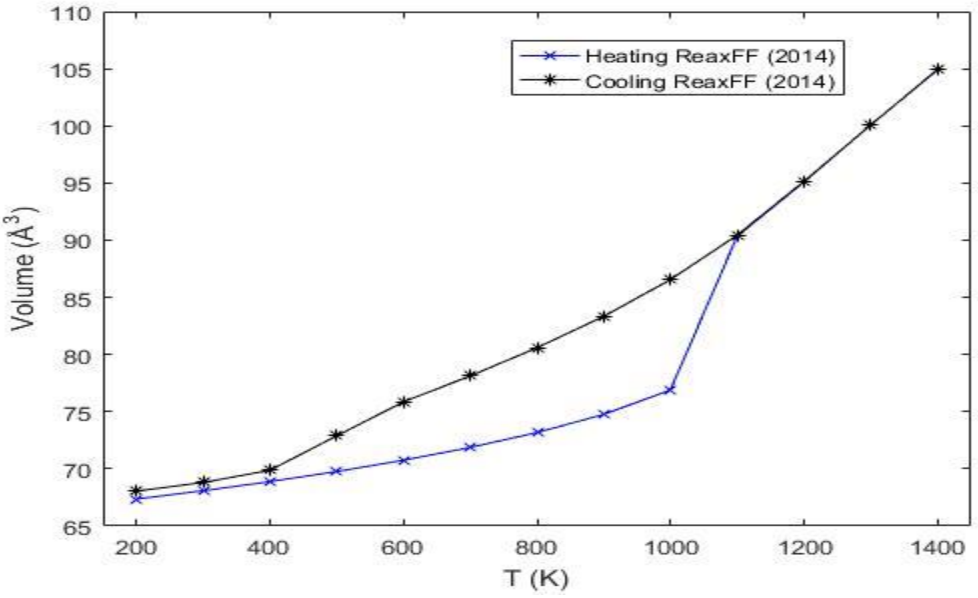

Figure 7: The temperature vs volume curves of aluminum heating and cooling simulations using ReaxFF (2014)

3.2.2.1. Cooling of Al_2O_3 and comparison with heating

When we compare the heating and the cooling simulations we observe 1.5 % difference between heating and cooling curves of alumina simulation using ReaxFF (2014), and the slopes of two curves are alike for volumetric thermal expansion on cooling and heating.

Figure 8 shows the temperature vs volume of unit cell for heating and cooling alumina simulations using ReaxFF (2014).

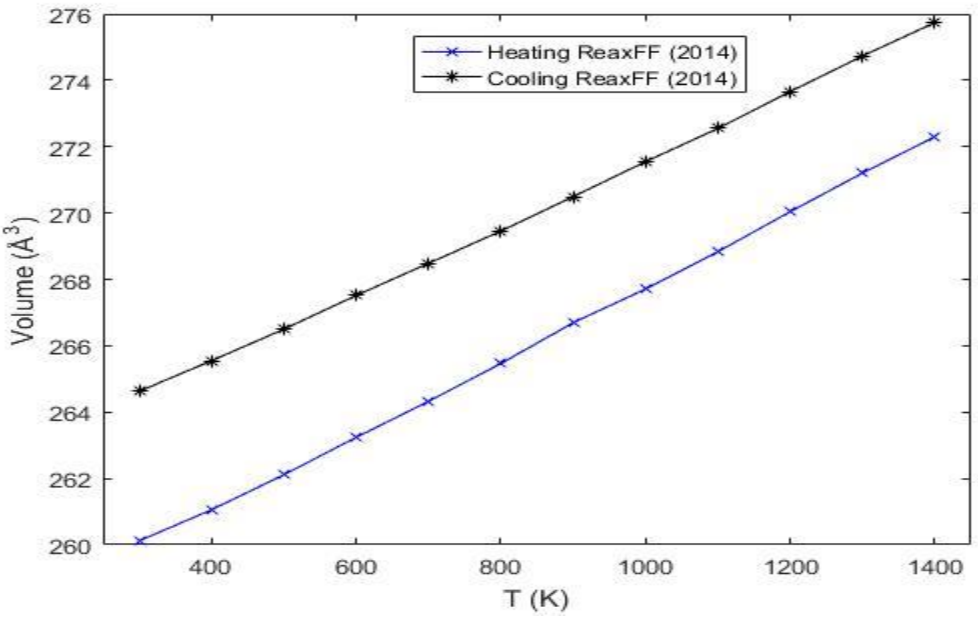

Figure 8: The temperature vs volume curves of Al_2O_3 heating and cooling simulations using ReaxFF (2014)

3.2.3. Heat capacity of Al and Al_2O_3

Heat capacity (specific heat) is defined as the energy needed to increase the temperature of system by one degree (see the Eq. 15). In our simulation, we have done a constant pressure simulation at different temperatures. Therefore, we can use the slope of temperature vs total energy curve to find the specific heat of the system.

$$C_P = \frac{1}{N}\left(\frac{\partial E}{\partial T}\right) \tag{15}$$

Figure 9 shows that the result of NPT heating up simulations for aluminum with three potentials which are the EAM, ReaxFF (2004) and ReaxFF (2014). The total energy of the system increases as a function of temperature. The values slopes of the curves are alike. However, the slope of ReaxFF (2014) is slightly larger than the slope of ReaxFF (2004) which in turn is marginally larger than the EAM. The sharp change of each curve represents the melting for the respective potential. Melting initiates at the same temperature for ReaxFF potentials, 300 K less than EAM potentials. Energy per mol values are similar in ReaxFF (2014) and EAM potentials.

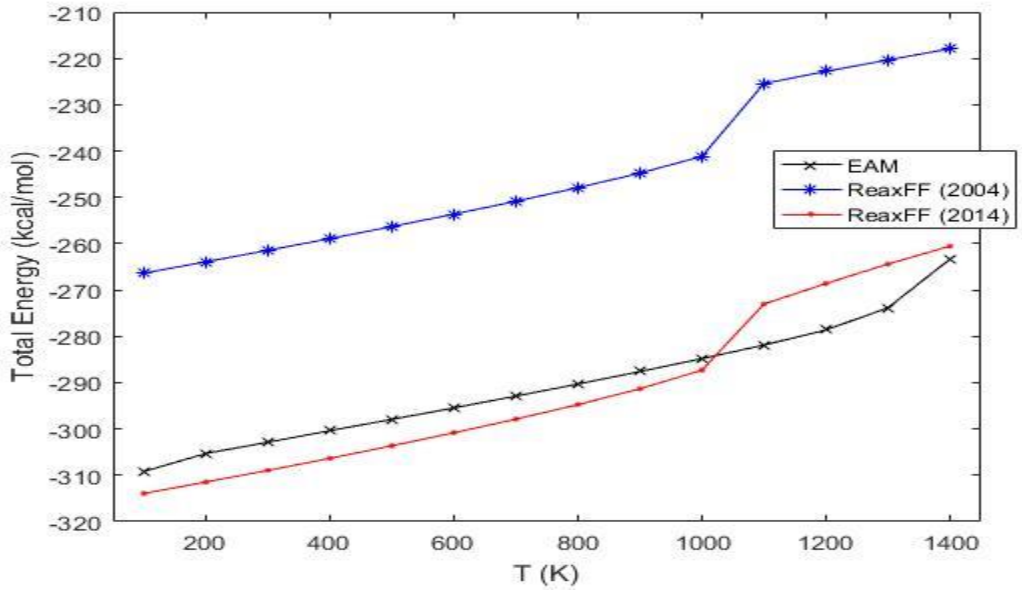

Figure 9: The temperature vs total energy curve of aluminum for EAM, ReaxFF (2004) and ReaxFF (2014).

Table 5 shows that the values of specific heat of aluminum and alumina found experimentally comparable with those of the values of our simulations using EAM, ReaxFF (2004) and ReaxFF (2014). Enthalpy of melting for both ReaxFF potentials are on the order of 16-17 kcal/mol.

Table 5: The specific heat of aluminum and alumina is listed for EAM, ReaxFF (2004) and ReaxFF (2014) potentials.

	Exp.	EAM (J/mol*K)	ReaxFF (2004) (J/mol*K)	ReaxFF (2014) (J/mol*K)
Al C_P	24.3[a]	26.29	28.8	30.4
Al_2O_3 C_P	79.4[b]	--------	125.3	123.2

[a] Reference [45]
[b] Reference [43]

3.3. Bulk Modulus of Al and Al_2O_3

Bulk modulus of material systems can be computed using NPT ensemble MD simulations by varying pressure over the isotherm. We performed simulations at 0.25, 0.5, 1, 2, 3, 4, 6, 8 GPa pressure and at different temperatures. We obtained our initial structures for bulk modulus simulations at the temperatures which are 100, 300, 500, 700 900 K, from the last position of heating up simulations at each temperature, respectively. Because heating up simulations are performed using NPT ensemble, and the pressure is constant at 0 bar. Therefore, we obtained the initial structures at 0 bar and different temperatures ranging from 100 K to 900 K. For example, we used the structure of heating up simulations at 900 K and 0 bar as an initial structure for bulk modulus calculation simulations for 900 K.

Bulk modulus (B) is the inverse of compressibility (χ) as formulated at eq. (8,17)

$$B = \frac{1}{\chi} \tag{16}$$

$$\chi = -\frac{1}{V_0}\frac{\Delta V}{\Delta P} \tag{17}$$

where V_0, ΔV, ΔP are initial volume, change in a volume and change in pressure, respectively.

3.3.1. Bulk modulus of aluminum using EAM, and ReaxFF

Bulk modulus of aluminum metal is calculated for 100, 300, 500, 700, 900 K using EAM, ReaxFF (2004) and ReaxFF (2014) potentials. We obtained bulk modulus values from pressure vs volume curve of bulk modulus simulations for different temperature from 100 K to 900 K. The experimental values of the bulk modulus of aluminum compared with the values obtained from the simulations which were performed with EAM, ReaxFF (2004) and ReaxFF (2014) is shown in Table 6.

Table 6: Bulk modulus of aluminum calculated with EAM, ReaxFF 2004 and ReaxFF 2014 for 100, 300, 500, 700, 900 K

T (K)	Exp.	EAM (GPa)	ReaxFF (2004) (GPa)	ReaxFF (2014) (GPa)
100	72[b]	114.1	92.4	71.83
300	75.7[a] 67[b]	110.8	87.7	64.25
500	72[a]	106.1	82.3	56.7
700	67[a]	99.4	75.8	48.7
900	62[a]	91.4	67.7	40.2

[a] Reference [46]
[b] Reference [47]

The bulk modulus values obtained by performing the simulations with the EAM, ReaxFF (2004) and ReaxFF (2014) have been compared to the reference values shown in Figure 10.

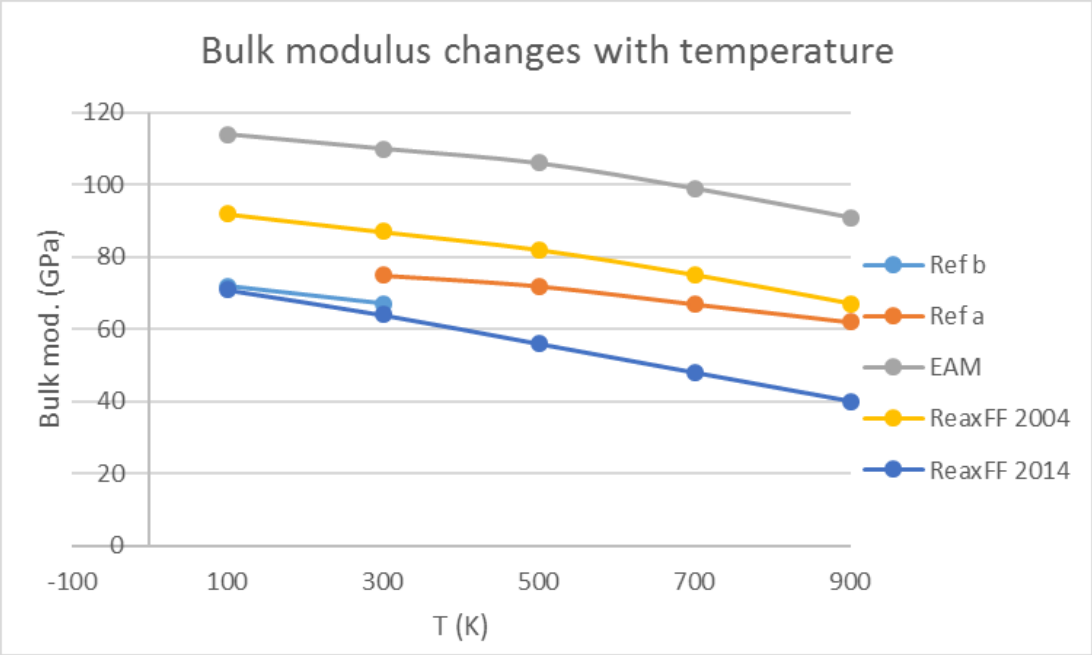

Figure 10: Comparison of bulk modulus values of aluminum temperature vs different potential. [a] Reference [46], [b] Reference [47]

The pressure vs volume curves obtained from the bulk modulus simulations with the EAM, ReaxFF (2004) and ReaxFF (2014) for different temperatures are shown in Figure 11. Additionally, we performed tensile modulus and compressive modulus simulations for aluminum using the potentials.

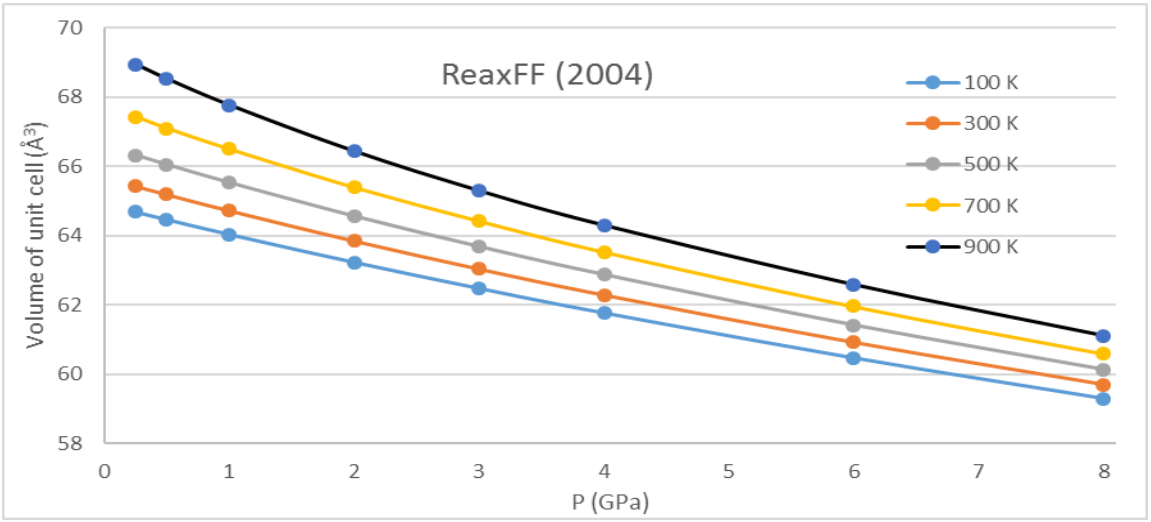

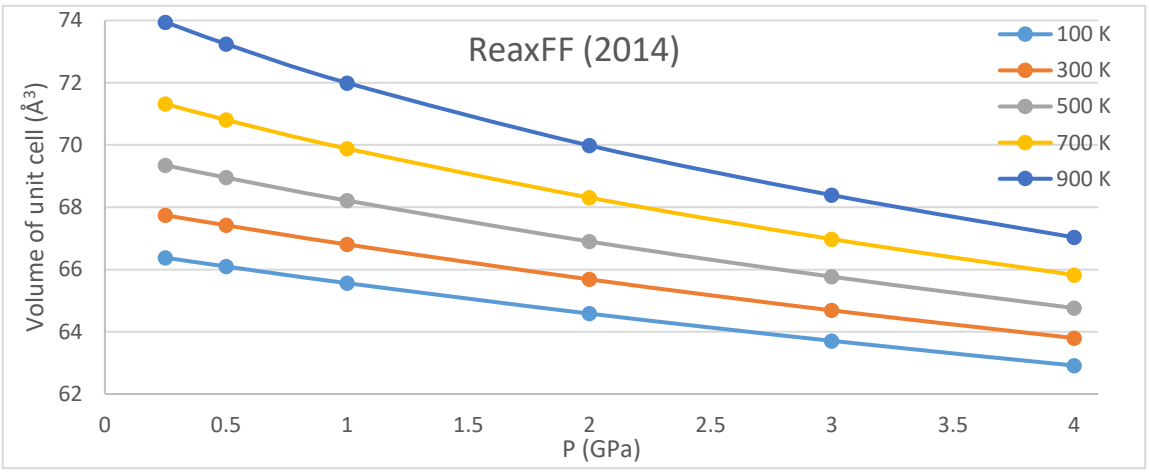

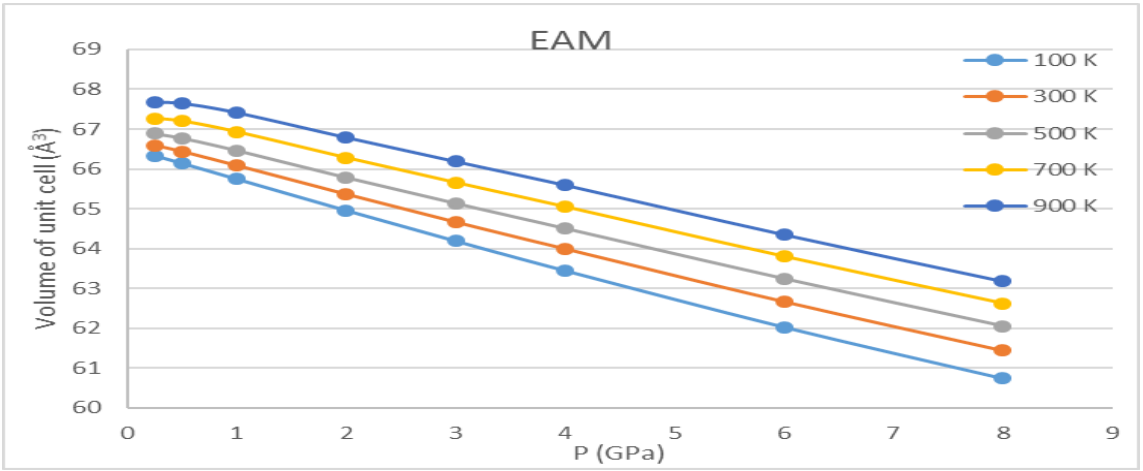

Figure 11: The pressure vs volume curves of aluminum for EAM, ReaxFF (2004) and ReaxFF (2014). First figure is ReaxFF (2004), second is ReaxFF (2014) and last one is EAM

3.3.2. Bulk modulus of alumina (Al_2O_3) using ReaxFF

We also calculated the bulk modulus of alumina at the different temperatures and with ReaxFF (2004) and ReaxFF (2014) potentials. The experimental values and simulations results are given in Table 7.

Table 7: Bulk modulus of alumina calculated with ReaxFF (2004) and ReaxFF (2014) for 100, 300, 500, 700, 900 K

T (K)	Exp.	ReaxFF (2004) (GPa)	ReaxFF (2014) (GPa)
100 K		200.9	259
300 K	252[a] 254[b]	194.5	246
500 K	247[a]	-	236
700 K	241[a]	-	232
900 K	235[a]	-	223

[a] Reference [48]

[b] Reference [49]

The pressure vs volume of the bulk modulus simulations of alumina for different temperatures with the ReaxFF (2004) and ReaxFF (2014) are shown in Figure 12.

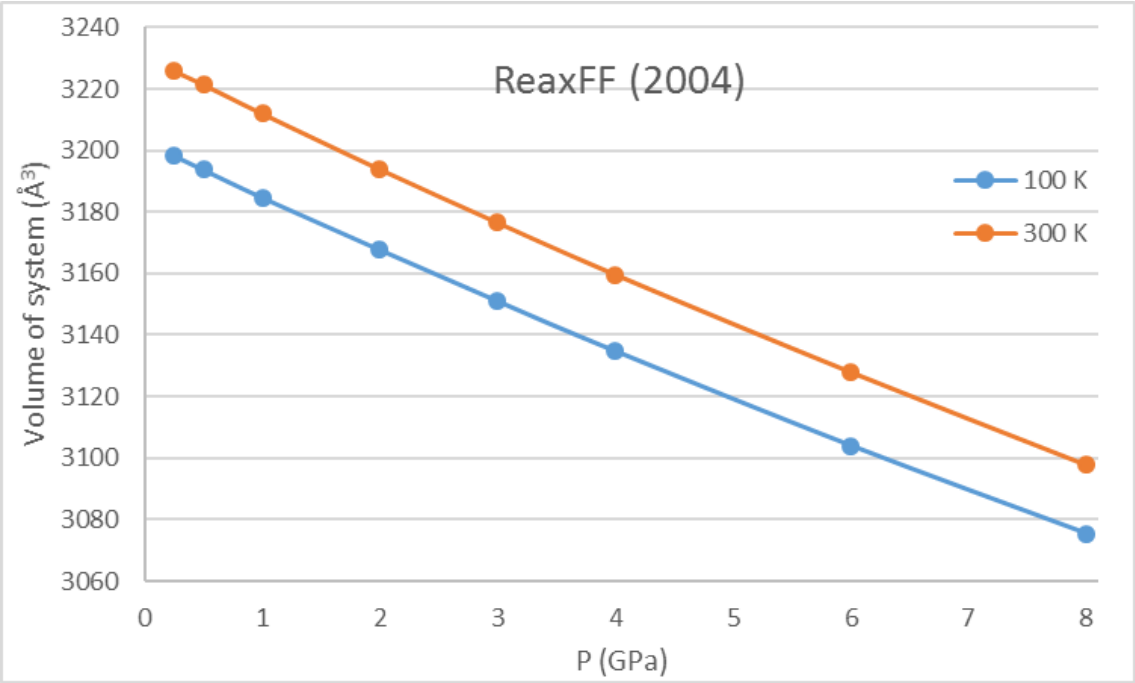

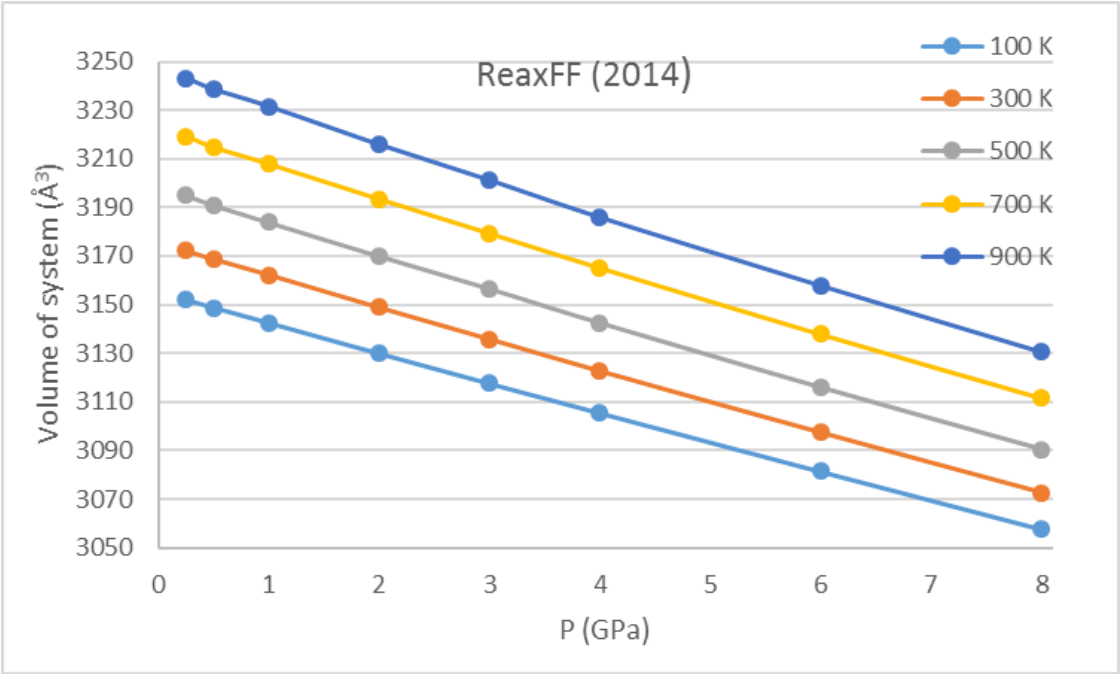

Figure 12: The pressure vs volume curves of alumina for ReaxFF (2004) and ReaxFF (2014) for different temperatures from 100 to 900 K. First figure represents volume vs pressure curve of ReaxFF (2004) for temperature 100 and 300 K. Second figure represent the volume vs pressure curve for ReaxFF (2014) from 100 to 900 K.

3.4. Structural Analysis

We studied structural properties of aluminum and alumina with EAM, ReaxFF (2004) and ReaxFF (2014) as a function of temperature. We employed pair correlation function (g(r), radial distribution function (RDF)) to investigate the structural correlations. RDF (g(r)) shows the density of atoms as a function of radial distance. Studying the pair correlation function at equilibrium simulations gives us assurance over the result of simulations for metal and alumina simulations (note that here we mean total pair correlation function for the compound). For alumina, we particularly calculated the partial radial pair distributions, $g_{AB}(r)$, where AB pairs are chosen as Al-Al, Al-O, O-O.

3.4.1. Aluminum RDF analysis

Figure 13 shows the radial pair distribution of Al-Al for the fcc aluminum simulation which is performed with ReaxFF (2004) for temperatures ranging from 100 to 1100 K. The first peak is at 2.80 Å which represents Al-Al bond length. Although the height of the first peak (intensity) decreases with the increasing temperature, the position of the first peak does not change drastically only representing very small shift to correspond thermal expansion. The decrease in peak height (intensity) is associated with a broadening as the temperature increased – a measure of increased amplitude of oscillation in bond length. Additionally, the first peak represents the nearest neighbors, and the second peak implies the second nearest neighbors and lattice parameters (4.05

Å) of the FCC aluminum structure. The integration of the area under 1st peak gives the first coordination shell (12) which is the number of the nearest neighbors in fcc crystal.

The density of the peaks decreases as a function of temperature. There is a small amount shift at the second and higher order peaks increasing with temperature. At 1100 K, a number of intermediate peaks disappear and merge into a low height peaks and shallow dips oscillating around 1, as indication of melting of Aluminum.

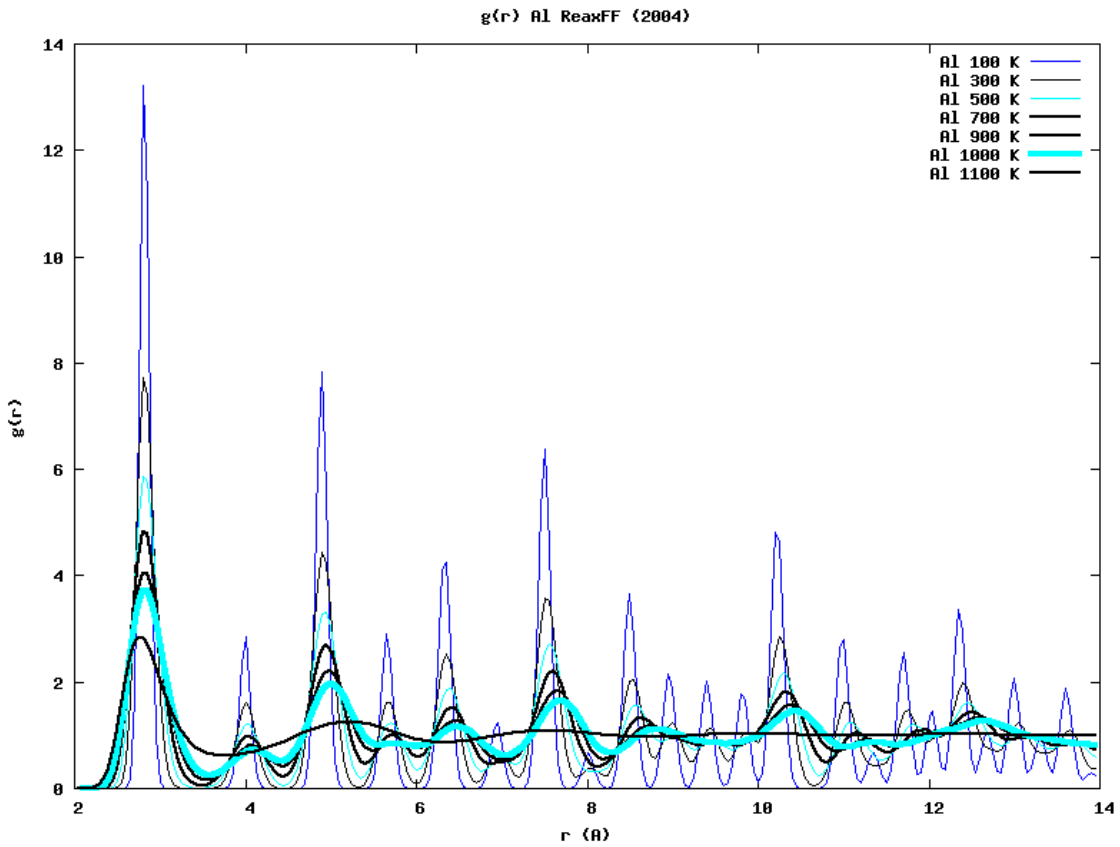

Figure 13: RDF of aluminum metal for ReaxFF (2004) for temperature from 100 K to 1100 K

We calculated RDF of Al-Al pair for ReaxFF (2014) and EAM potentials. Figure 14 shows the RDF of ReaxFF (2014) from 100 K to 1100 K, and RDF plots of aluminum simulations performed with ReaxFF (2014) and ReaxFF (2004) are alike. Figure 15 shows the RDF of EAM potential upto 1400 K. EAM potential results reveals the fact that Aluminum stays solid almost up to 1300 K.

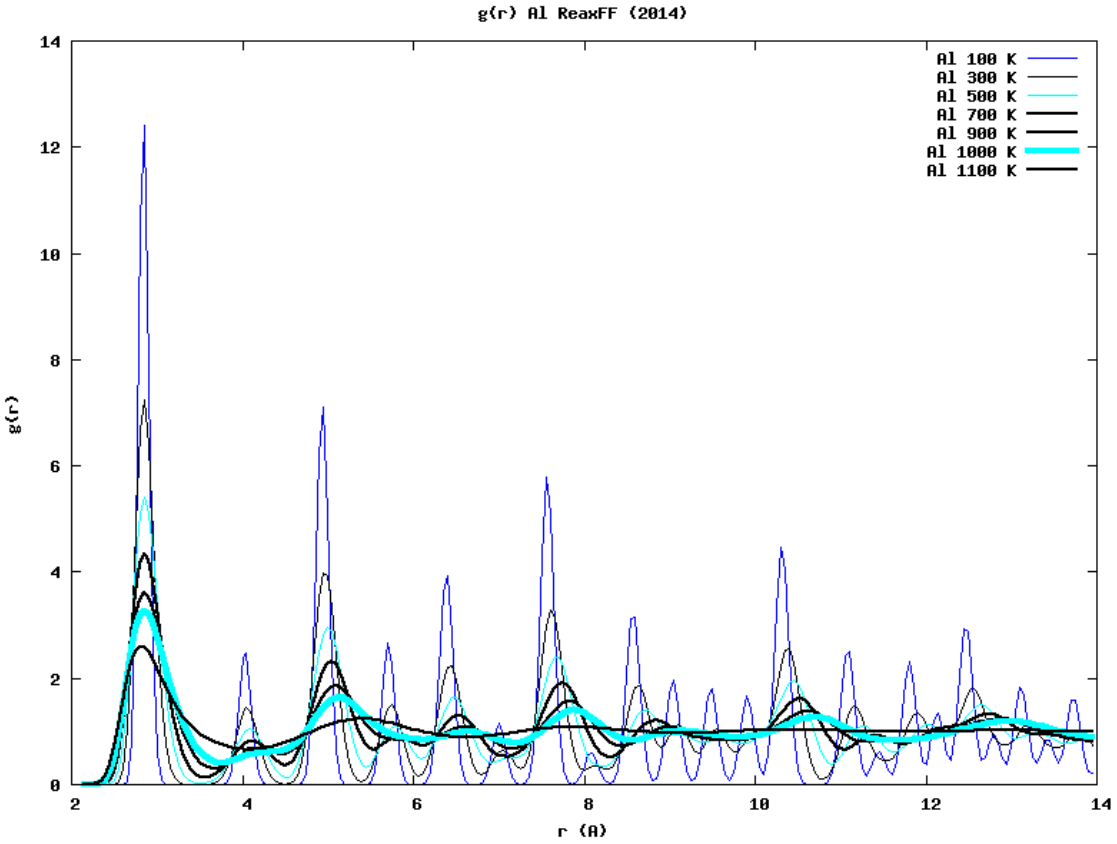

Figure 14: RDF of aluminum metal for ReaxFF (2014) for temperature from 100 to 1100 K

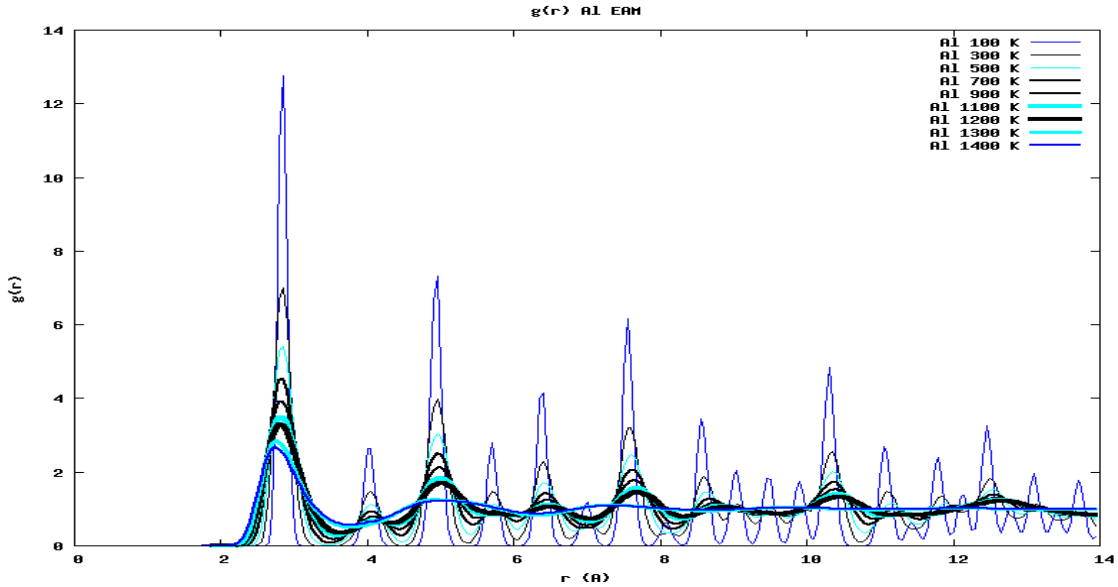

Figure 15: RDF of aluminum simulations for EAM potential at different temperatures from 100 K to 1400 K. RDF curves of 1300 K and 1400 K simulations are nearly same because aluminum metal melted at 1300 K for EAM.

3.4.2 Alumina RDF analysis

We studied the structure of alumina at temperatures 0, 100, 500 K using radial distribution functions to assess the structural aspects resulting from two different ReaxFF potentials. Partial radial distribution functions for Al-Al, Al-O and O-O pairs by employing ReaxFF (2004) and ReaxFF (2014) potentials are plotted in Figure 16. The first strong peak is at r=1.90 Å for Al-O pairs at 100 K and 500 K. However, 0 K represents the initial structure of the alumina heating simulations. Therefore, there are two impulses at r=1.85 and 1.95 Å instead of the peak at 1.90 Å. The second and third order peaks become smooth at higher temperatures.

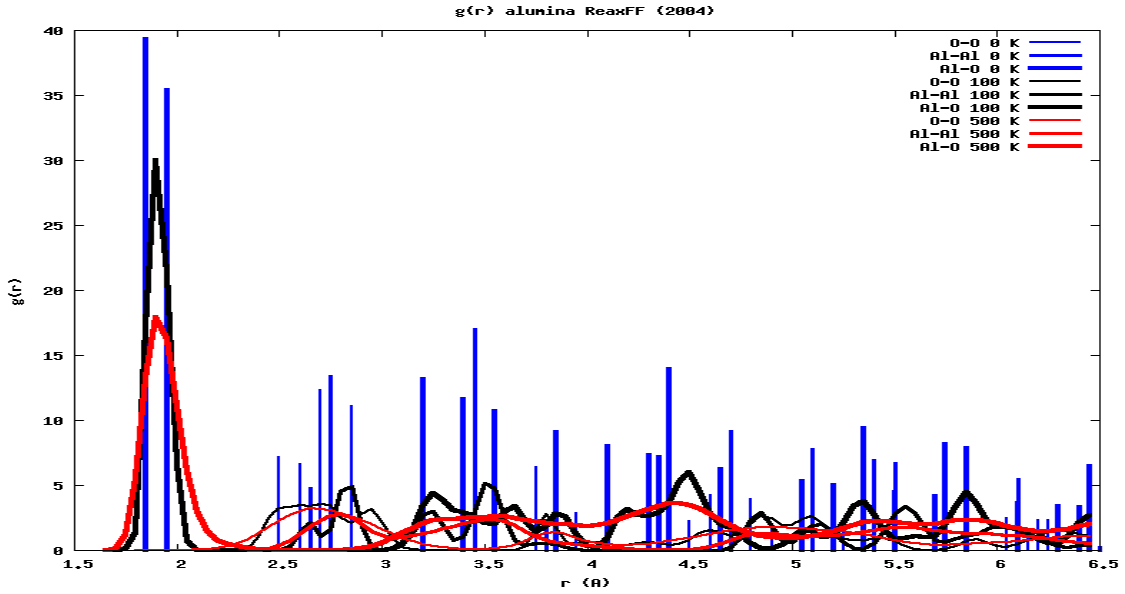

Figure 16: RDF of Al-O, Al-Al, O-O pairs in alumina simulations for ReaxFF (2004) potential for 0 K, 100 K and 500 K.

We also studied RDF of alumina heating up simulations for Al-Al, Al-O and O-O pairs with ReaxFF (2014). Figure 17 shows the Al-Al, Al-O and O-O pair correlations at alumina heating simulations with ReaxFF (2014). As mentioned previously, 0 K represents the initial structure of alumina heating simulations. Similar to ReaxFF (2004) alumina heating up simulation, there are two impulses at r=1.85 and 1.95 Å instead of the peak at 1.90 Å. However, the first strong peak is at r=1.90 Å for Al-O pairs at 100 K, 500 K. The second and third order peaks become smooth at higher temperatures.

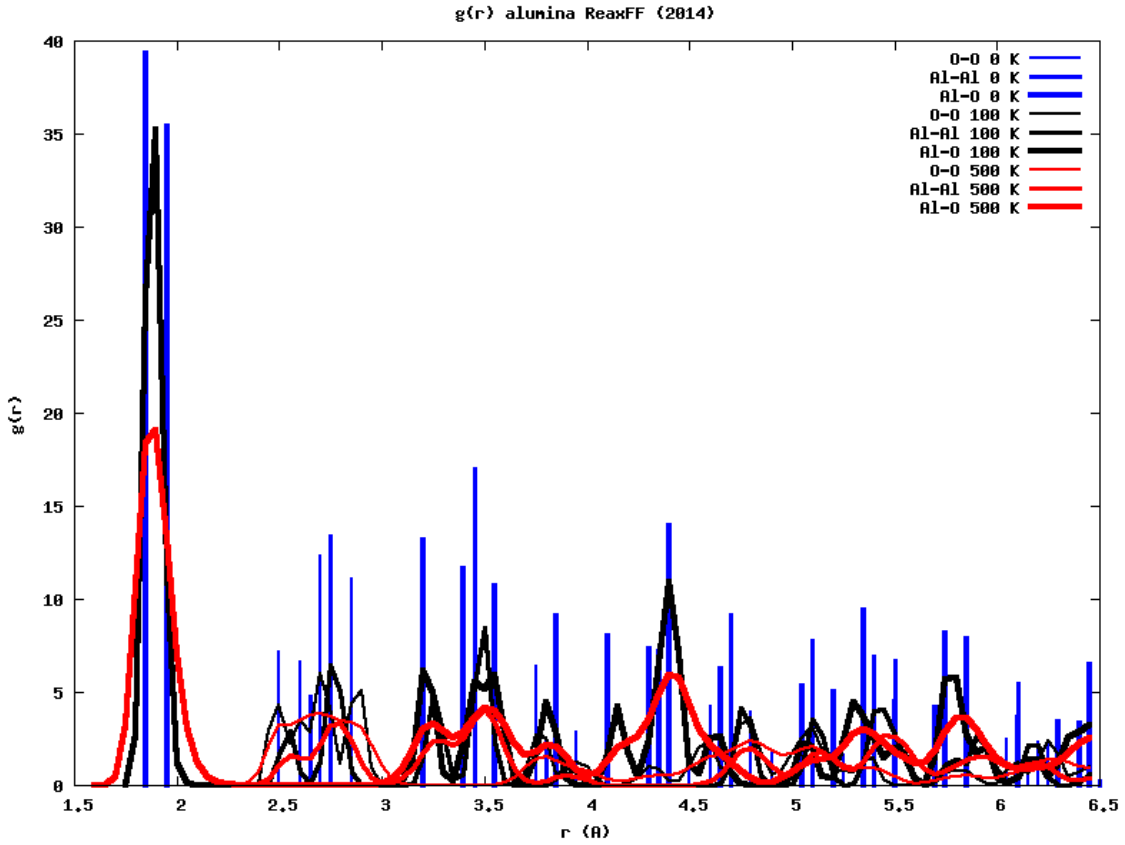

Figure 17: RDF of alumina simulations for ReaxFF (2014) potential for 0 K, 100 K and 500 K.

4. WETTING AND SURFACE FORMATION ENERGY SIMULATIONS

Surface science is very crucial in understanding the interactions between liquid droplet and solid surface such as adhesion, wetting and non-wetting. Surface science has been used to understand where surfaces of materials play a critical role in overall properties such lubricants, inter-material binding and adhesion, inter-phase interactions and solid-liquid interactions [50]. As an example, improvement of solid-liquid interactions is significant for many industries such as coating, production of paints, textiles and petroleum.

Solid-liquid interactions can be defined using wetting concept as described by Young in 1805 [51]. Wetting is defined from the angle at air, liquid, solid interface where mechanical equilibrium among liquid-gas (σ_{lv}), solid-liquid (σ_{ls}) and solid-gas (σ_{sv}) interfacial free energy (Figure 18, eq18).

$$cos\theta = \frac{\sigma_{sv} - \sigma_{ls}}{\sigma_{lv}} \tag{18}$$

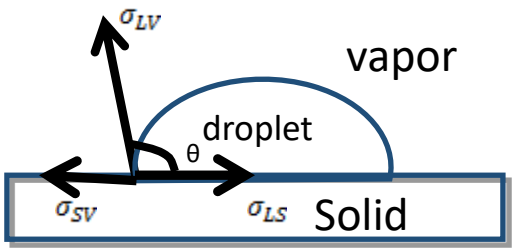

Figure 18: Schematic drawing for macroscopic droplet and contact angle.

In general, wetting can be categorized into: static and dynamic wetting. In static wetting, the parameter, contact angle defining the wetting behavior of material, doesn't change in time. On the other hand, at dynamic wetting, it changes as a function of the time.

4.1. Surface Free Energy

In bulk materials such as a pure gas, liquid, or solid system, atoms experience same amount of forces in all directions from the surrounding atoms, as the name ‘bulk’ implies insignificant surface/interface effects. However, at solid-liquid, liquid-gas and gas-solid interfaces, there are unbalanced forces that exist because of difference in energy of the interacting atoms from different phase [52]. The difference in density, attractive and repulsive energies between two phases cause the extraction of molecules into the phase which has stronger attractive force such as gas to liquids as shown in Figure 19 or the opposite attract the molecules/atoms from the low-density phase to solid substrate.

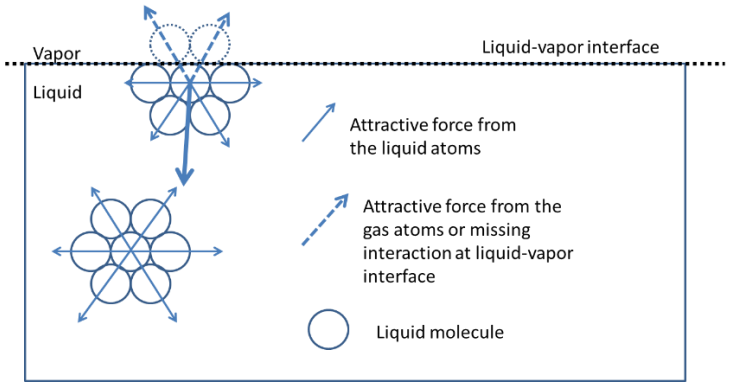

Figure 19: Schematic draw for effective force on an atom in liquid and liquid and vapor interface after Taherian 2013 [52].

As interfaces and interface formation is dictated by the surface free energy, a thermodynamic discussion becomes pertinent. Change in Gibbs free energy, which is a thermodynamic variable, at constant volume, temperature and number of particle (NVT) conditions depend on interface area is defined as surface free energy. Gibbs free energy is given at equation (19).

$$dG = -SdT + PdV + \sum \mu_i dN_i + \sigma dA \tag{19}$$

where S, T, V, P, N, A, σ, μ are the entropy, temperature, volume, pressure, number of atom, area of interface, surface free energy, chemical potential, respectively.

As we know from thermodynamics, a material system always tends to transition to a lower free energy state. Surface free energy will contribute to increase in the system's free energy as it can be seen in equation (19) where the surface free energy is dependent on the interfacial area. Therefore, any system will try to decrease their surface area as

physically permissible. As an example, water molecules inside vapor gets more spherical as a sphere has the smallest geometrical surface area in comparison to other geometrical shapes. In addition, in any two liquids that have a very large surface tension difference, the higher surface free energy liquid prefers to shape itself into a sphere.

4.2. Contact Angle

Wettability of liquid droplet on the solid substrate can be defined using the concept of contact angle. The contact angle measurement is essential in surface science and wetting studies because the contact angle has a direct relationship with the surface free energy. When a lower contact angle is measure, it is understood that the interface has a higher surface energy and therefore, has higher wettability.

The contact angle of liquid-solid system at macroscopic level can be defined using a sessile drop technique. In this technique, purified liquid is dispensed onto a properly cleaned solid surface. Solid surface and liquid droplet have to be physically and chemically non-reactive. The solid surface has to be horizontal optically because contact angle is captured by optical devices [50].

Using the technique above, one can measure both the static and dynamic contact angle. Static contact angle can be defined by using surface free energies of air-liquid-solid interfaces. To define contact angle θ, Young's equations use mechanical equilibrium among liquid-gas (σ_{lv}), solid-liquid (σ_{ls}) and solid-gas (σ_{sv}) interfacial free energy (Figure 18).

4.3. Calculation of Contact Angle

The concept of contact angle can be used to describe degree of wetting at liquid solid interface. As we described above, macroscopic parameter of contact angle can be measured accurately employing sessile drop method. However, traditional contact angle methods may not be enough to describe at the microscopic level such as molecular dynamic calculations, as shown at Figure 20 also see and compare Figure 18. We need more general description to calculate the contact angle of microscopic droplet and MD simulations. Therefore, we can compare more accurately the result of MD simulations and experimental measurements. Hautman and Klein[53] present an approach to calculate the contact angle of irregular micro droplet.

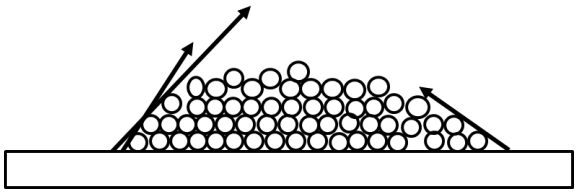

Figure 20: Schematic drawing of microscopic droplet. Traditional methods may mislead after Fan&Cagin 1995 [55].

The liquid-solid surface tension cannot be directly derived from the contact angle. Therefore, we need contact angle to define and derive surface free energy of materials. Each frame of MD trajectory defines the momentary contact angle. Hence, a relationship between R and H is needed to calculate the contact angle for MD simulations. Equation 2 describes the relationships of each parameter on Figure 21 where R, R_0, θ and H are

radii of the spherical droplet, contact angle and height of droplet, respectively. While R and H can be found from experimental or simulation result, R_0 is determined using (20) [54]

$$\theta = tan^{-1}\left(\frac{R}{R_0 - H}\right) \text{ and } R_0 = \left(\frac{R^2}{H+H}\right) \quad (20)$$

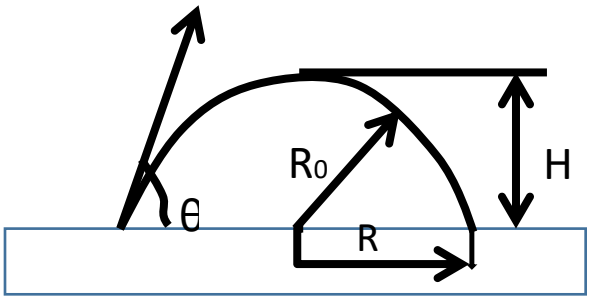

Figure 21: Schematic drawing of parameter H, R, θ and R_0

Hautman and Klein[53] present an approach to calculate contact angle of micro scale droplet using geometric parameters which are employed for irregular and spherical shape. Here, Fan & Cagin [55] outline general connection between parameters such as height (h) & radius (r) and contact angle (θ) of a droplet. We assume the droplet as an intersected sphere for simplicity (see Figure 22). Figure 22a shows spherical droplet with contact angle lower than 90º (θ<90º), and 22b shows a droplet with contact angle greater than 90º (θ>90º).

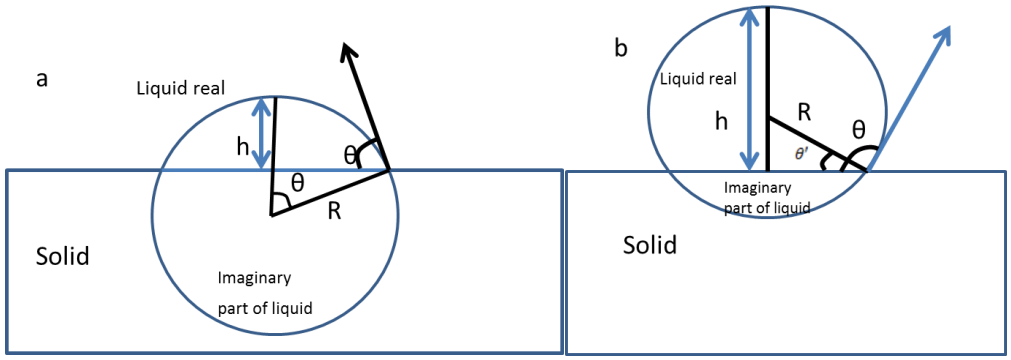

Figure 22: Schematic drawing of contact angle for intersected sphere a) contact angle lower than 90º and b) θ higher than 90º after Fan&Cagin 1995 [55].

In Figure 22, θ>90 $\cos\theta = \frac{(R-h)}{R}$ similarly for fig b, θ<90 $\cos\theta = -\sin\theta' = \frac{-(h-R)}{R}$. Therefore, contact angle of a system can be defined as $\cos\theta = 1 - \frac{h}{R}$. Volume and interfacial area of the droplet might be employed to calculate h and R in the system. In equation 5, V_d (see (21)) is volume, A_i(see (22)) is interfacial area and r_i is interfacial radius of droplet (see Figure 23).

$$V_d = \frac{\pi h(3r^2 + h^2)}{6} \tag{21}$$

$$A_i = \pi r^2 \tag{22}$$

$$R^2 = (R-h)^2 + r^2 \tag{23}$$

$$h^3 + \frac{3A_i}{\pi}h - \frac{6V_d}{\pi} = 0 \tag{24}$$

$$R = \frac{h}{2} + \frac{S}{2\pi h} \tag{25}$$

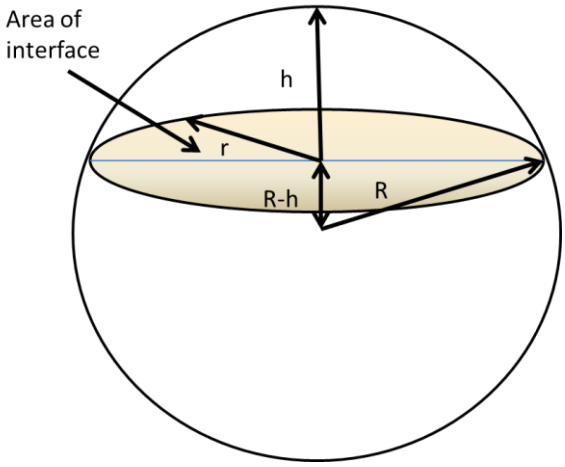

Figure 23: Schematic drawing for volume and interface area of droplet after Fan&Cagin 1995 [55].

For any size and shape of the droplet, volume (V_d) and interfacial area (A_i) can be calculated from simulation's trajectory file for each time step. We employed the above recipe to determine quantity of surface wetting for microstate position at any time step.

A 3D grid is employed to calculate the volume of wetting simulation. If a position of the atom is within the grid, we assume it is occupied. Also an interior unoccupied position which has no direct connection to outside will be counted as occupied volume. To calculate volume of droplet, we summed all the occupied sides of the grid. If an unoccupied system come across an occupied grid in all three dimension (x, y, z), the interior unoccupied grid is counted as an occupied grid and will contribute the volume of droplet. Wetting surface of the simulation is calculated perpendicular to z direction. A two-dimensional grid is constructed to calculate wetted surface.

In our studies, we choose to use a method which developed by Hautman and Klein[53], equivalent though simpler than Fan and Cagin method [55]. In this approach,

the contact angle calculated from micro scale droplet using geometric parameters which we mentioned.

$$z_{c.m} = (2)^{\frac{-4}{3}} R_0 \left(\frac{1-\cos\theta}{2+\cos\theta}\right)^{1/3} \frac{3+\cos\theta}{2+\cos\theta} \quad (26)$$

where $z_{c.m}$ is measured center of mass, R_0 radius of free spherical droplet (initial radius of droplet) and θ is contact angle of droplet.

4.4. Surface Formation Energy of Al and Al_2O_3

The surface formation energy of Al/Al and Al_2O_3/Al_2O_3 interfaces is studied for different temperatures and potentials which are EAM, ReaxFF potentials. Simulations are performed under vacuum conditions and without vapor pressure effect for both aluminum and the alumina system. Detailed information is provided in the following sections because two slightly different methods are used for Al/Al and Al2O3/Al2O3 interfaces.

Surface formation energy can be described as an energy required to create a new unit surface from bulk materials due to breaking of bonds between two slabs. It is an isotropic property of the material. Therefore, the surface formation energy density of the materials is depended on the crystalline plane of single crystal. Surface formation energy of the material can be calculated with following equations

$$\Delta E_{surf} = \frac{(E_{sl1}^{tot} + E_{sl2}^{tot} - E_{bilayer}^{tot})}{2A} \quad (27)$$

where A, ΔE_{surf}, E_{sl1}^{tot}, E_{sl2}^{tot}, $E_{bilayer}^{tot}$ are interfacial area, surface formation energy, internal energy of slab 1, slab 2 and bilayer (two slab together) respectively.

4.4.1 Surface formation energy of Al_2O_3

To calculate surface formation energy of Al_2O_3, we employed two steps of MD simulations using ReaxFF (2014) and ReaxFF (2004). First, we create 4x3x1 Al_2O_3 crystal, and performed heating simulations using NPT ensemble up to 1400 K with an increment of 100 K. In the second step of surface formation energy calculations, the NPT (isothermal-isobaric) simulation is switched to NVT (canonical ensemble) to create slabs from bulk materials with exactly the same thermodynamic properties. The initial structure of the NVT simulations are obtained from the last frame of the NPT simulations. However, averaged volumes of heated system are chosen for the second step MD simulations of surface formation energy. Therefore, atomic configurations of the last frame of NPT simulations are adjusted to average volume and position of equilibration simulations (shown in eq. (28,29))

$$V_a = \frac{L_{xi*}L_{xa}}{L_{xi}} * \frac{L_{yi*}L_{ya}}{L_{yi}} * \frac{L_{zi*}L_{za}}{L_{zi}} \tag{28}$$

where V_a, L_{xi}, L_{xa} are average volume, instantaneous length and average length, respectively.

$$P_a = \frac{P_i L_a}{L_i} \tag{29}$$

where P_a, P_i, L_i, L_a are average and instantaneous position, instantaneous length and average length, respectively.

The average volume crystal structure is replicated and translated with distance (z+x) from the original positions along (0001) directions, where z is c lattice parameters and x is vacuum distance, changing from 5 to 20 Å at the simulations. Vacuum between two slabs enables the crystal structure to expand or contract within the simulation box, that's the relaxation of surfaces. NVT simulations are performed with periodic boundary condition at each direction. Therefore, two new surfaces are created on bulk crystal to calculate surface formation energy of Al_2O_3. Figure 24 shows the Schematically representation of NPT and NVT simulations of surface formation energy calculations for alumina ceramics using ReaxFF (2004) and ReaxFF (2014).

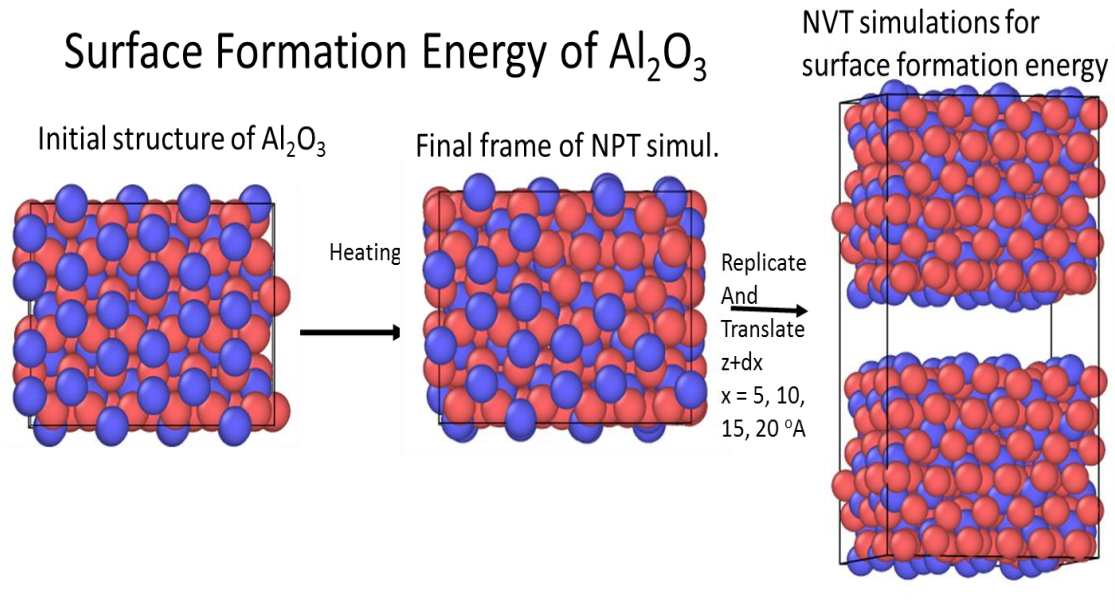

Figure 24: Schema of surface formation energy calculation for Al_2O_3

Next, NVT simulations are performed with four different vacuum thicknesses 5, 10, 15, 20 Å, between of two alumina slabs. Figure 25 shows snapshots of the last frame of alumina simulations performed with ReaxFF (2014) potential for 4 different vacuum distances in the middle of slabs.

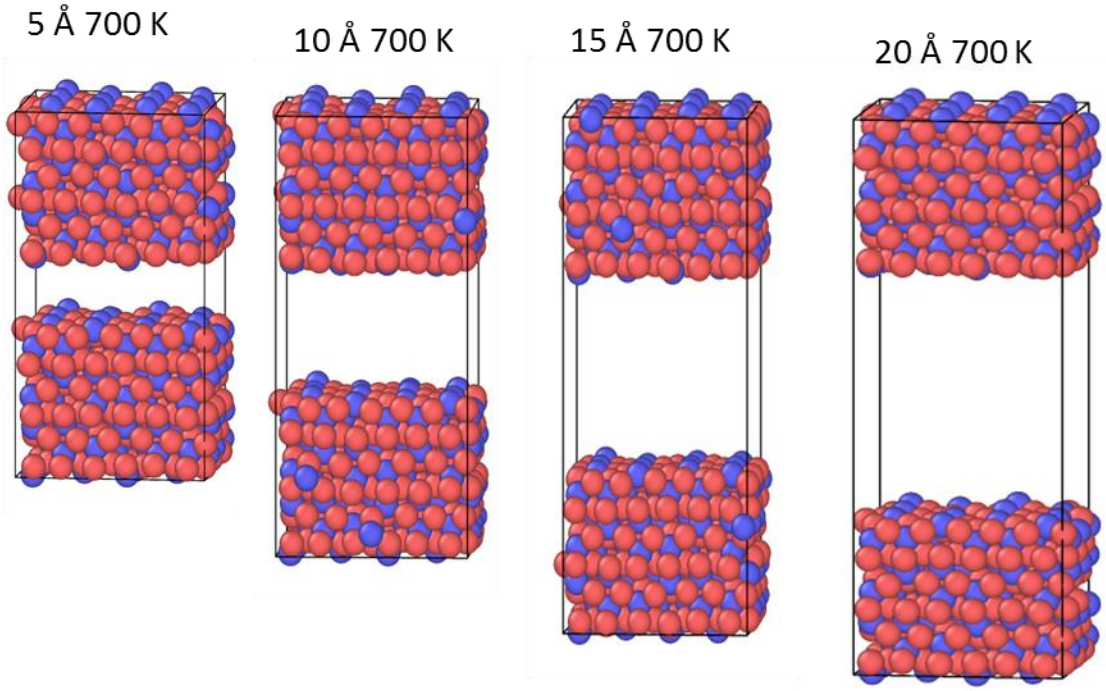

Figure 25: Snapshot of last frame of NVT simulations for four different vacuum thickness at the 700 K.

4.4.2. Surface formation energy of aluminum

To calculate the surface formation energy of aluminum, the same two steps (successive NPT and NVT ensemble MD simulations) of alumina simulations are followed. However, while creating the initial structures of NVT simulations, we

apply slightly different method vs the alumina simulations. The only difference is the crystal structure is separated in the middle of z lateral site and translated a vacuum distance (x) at (001) directions instead of replicate and translate.

NPT simulations are performed with a super cell of 10x10x10 unit cells (4000 atoms) using the 3 different potentials. Last frame of equilibration simulations are used as the initial configuration of NVT simulations ranging from 700 K to 1400 K with the increment in temperatures chosen as 100 K. Positions of atoms in the last frame of NPT simulations are adjusted to the average volume of the equilibrium simulations using eq. (28,29). The NPT aluminum simulation structures are separated in the middle of z lateral site. Therefore, two10x10x5 slabs are created. One of the slaps is translated 5, 10, 15, 20 Å at (001) directions to create vacuum between slabs. the new structure is used as an initial structure of NVT simulations. Figure 26 shows procedure of surface formation energy simulations for aluminum.

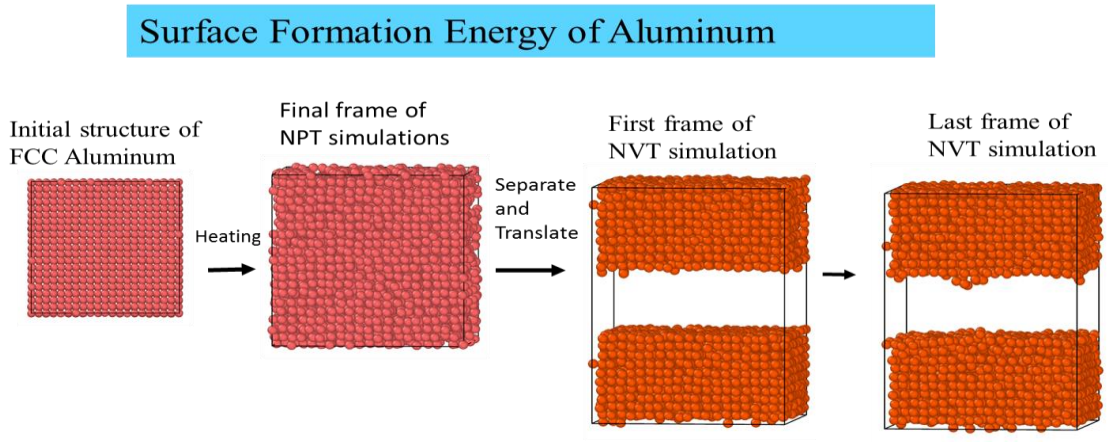

Figure 26: Schema of procedure of surface formation energy calculation for aluminum

4.4.3. Results of surface formation energy simulations

The temperature and total energy curves of NPT and NVT simulations are compared in Figure 27. 0 Å represent NPT simulations, which has the lowest energy since there is no vacuum between two slabs. 5 Å, 10 Å, 15 Å and 20 Å represent the NVT simulations with vacuum in the middle of slabs. The total energy of the NVT simulations with respect to different temperature are similar to each other. However, 0 Å simulations results is the lowest energy among the 5 different simulations. Because creating new surface requires energy to break bonds between Al-Al and Al-O.

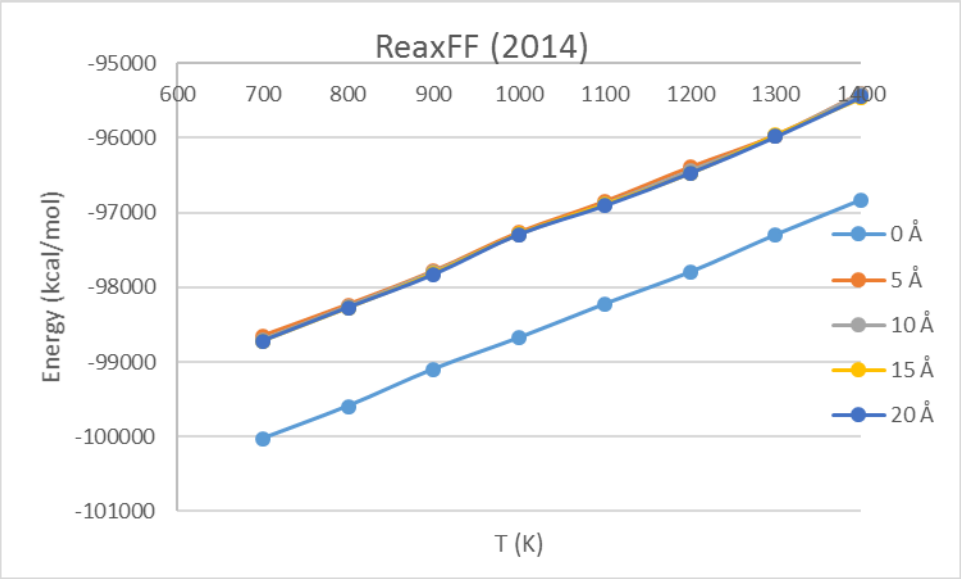

Figure 27: The temperature vs total energy curves of surface formation energy simulation for Al_2O_3 with 0, 5, 10, 15, 20 Å vacuum between two slabs using ReaxFF (2014)

The surface formation energy of Al_2O_3 was calculated using ReaxFF (2014) for four different separation distances at different temperatures. Figure 28 shows the energy vs separation distance curve. The energy converges with increasing separation distance. Therefore, surface formation energies are calculated for 20 Å which is assumed as an equilibrium distance.

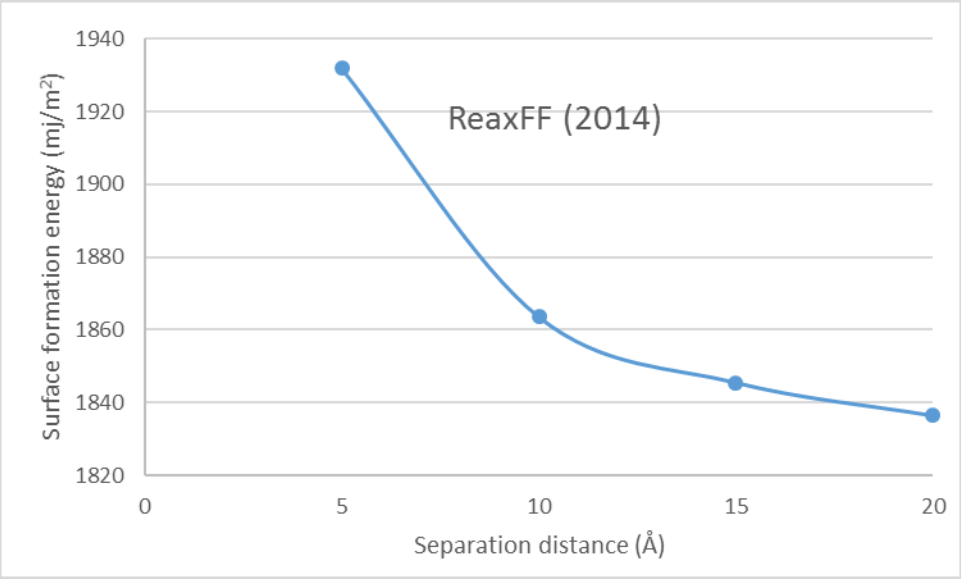

Figure 28: The separation distance (Å) vs surface formation energy curves for 700 K simulations performed with ReaxFF (2014). Curves shows that the surface formation energy converge at 15 and 20 Å.

The temperature and total energy curves of NPT and NVT aluminum simulations using ReaxFF (2004) potential are compared (shown in Figure 29). 0 Å represents NPT simulations, which is at the lowest energy because there is no vacuum between two slabs. 20 Å represent the NVT simulation, which have a 20 Å vacuum distance in the middle of the slabs. Energy of NVT simulations show similar result with respect to the

temperature variations due to vacuum between slabs. However, there are larger differences between energy curves of NVT and NPT (0 Å) simulations due to surface formation energy. Furthermore, the energy differences are even larger at the 1000 K. This large energy difference is mainly due to the melting process of aluminum at these temperatures for ReaxFF (2004). The three potentials show similar melting processes in the presence of surface in these surface formation energy simulations.

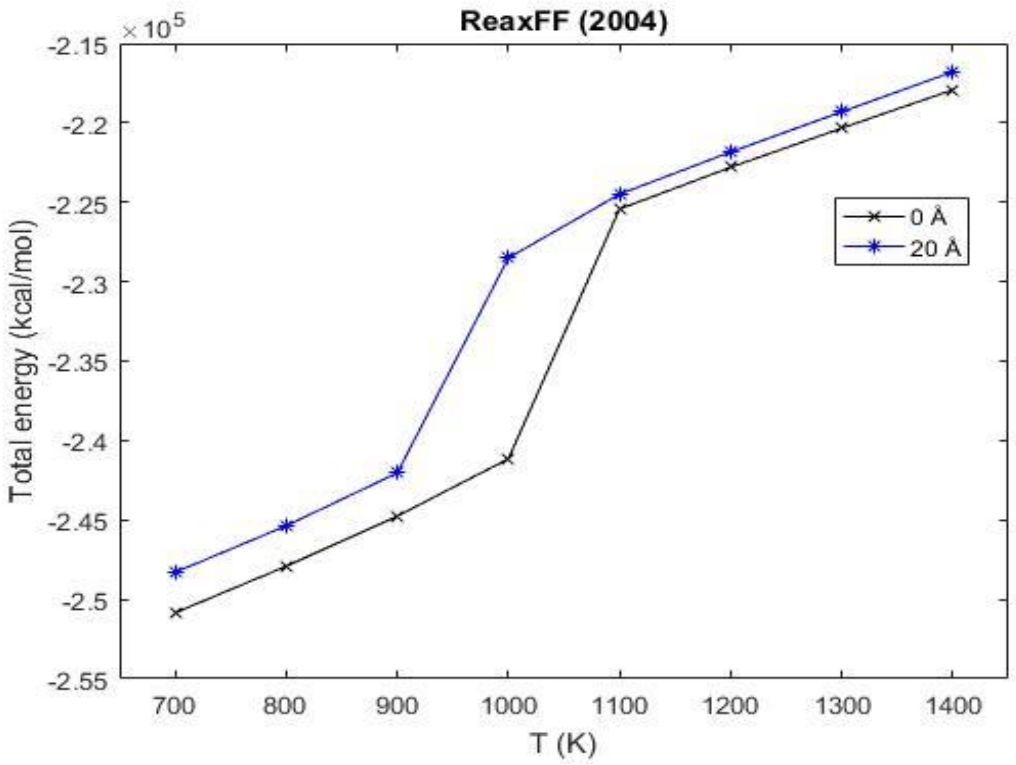

Figure 29: The temperature vs. total energy curves of surface formation energy simulation for aluminum using ReaxFF (2004).

There are two important phenomena during the melting process which cause the energy difference at 1000 K (shown in Figure 29). First, the enthalpy and total energy of materials are increasing during the melting process. Second, the melting process initiates from the surface of materials and progresses into the material system. However, in MD simulations with periodic boundary condition, melting points resulting from the bulk material simulation is higher than actual melting points due to lack of surfaces, yields with higher values than experiments, i.e. super heating.

In surface formation energy simulations, we create free surfaces via creating a vacuum in the middle of aluminum fcc crystal structures. Therefore, there is no periodic boundary effect on the two new surfaces. The melting process starts from free surfaces and progresses into the system. Consequently, melting occurs at a lower temperature than NPT simulations predict (used periodic boundary conditions without a free surface in the middle). Figure 30 shows the snapshots of surface formation energy simulations at 1000 K with 20 Å vacuum gap using ReaxFF (2004) for different time. The 1000 K NVT simulation shows that aluminum melted. However, NPT the simulation indicates that the melting temperature of aluminum using the EAM potential is 1300 K.

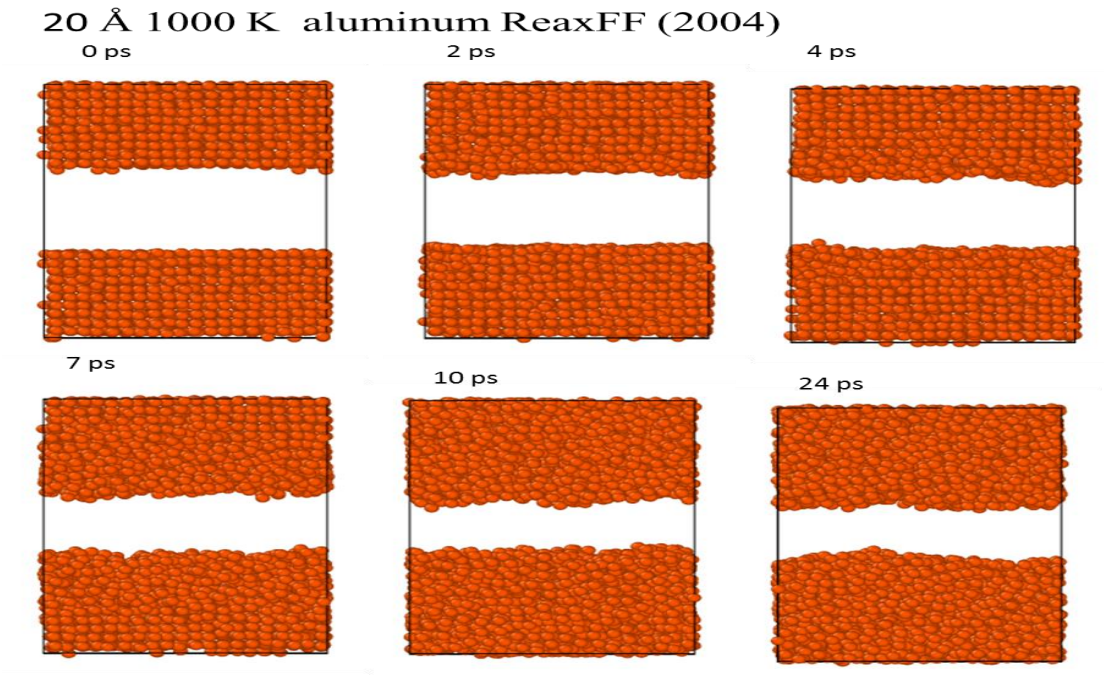

Figure 30: Snapshots of surface formation energy simulations at 1000 K with 20 Å vacuum using ReaxFF (2004). 0 ps shows very crystal structure, however disorder start from two free surface and progress along z directions as a function of time. Finally, aluminum melt (see 24 ps)

Figure 31 shows the temperature vs surface formation energy of aluminum simulations using ReaxFF (2004) at 20 Å and the temperatures range from 700 K to 1400 K. There are coherence surface formation energies (around 530 mj/m^2) at 700, 800 and 900 K. However, there is a very strong peak at 1000 K which indicates there is melting at aluminum at the temperature.

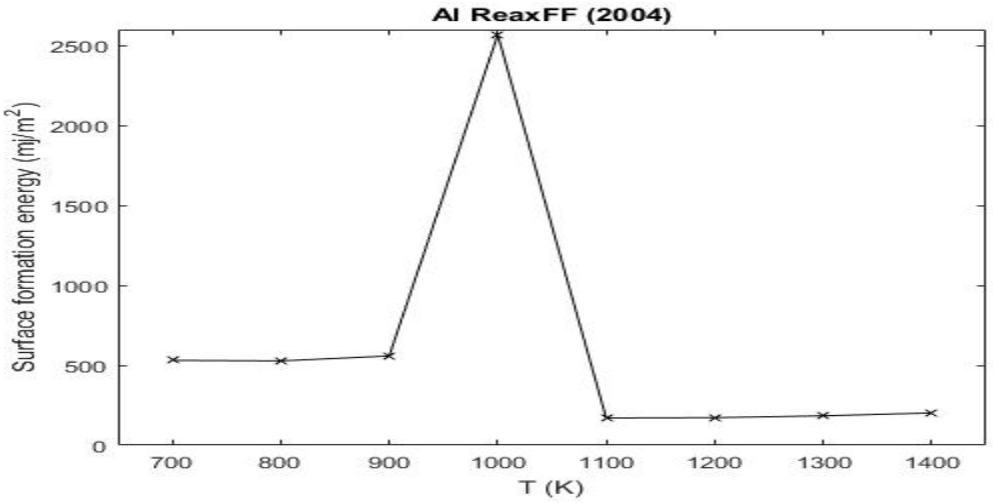

Figure 31: The surface formation energy of aluminum for temperatures at 20 Å separation and from 700 to 1400 K using ReaxFF (2004) potentials. There are clear difference energies at the temperatures 1000 K. The difference indicates that there is melting at that temperatures.

Surface formation energy simulations are performed with EAM, ReaxFF (2004) and ReaxFF (2014) potentials for aluminum and alumina. Table 8 shows the surface formation energy of Al and Al_2O_3 at 700 K employing EAM, ReaxFF (2004) and ReaxFF (2014) potentials. The calculated surface formation energies from the ReaxFF and EAM potentials are compared with experimental surface energies in the literature. All three potentials underestimated the surface energy

Table 8: The surface formation energy values of alumina and aluminum for the potentials at 700 K and with 20 Å separation distance between slabs. Experimental values are surface energy of FCC Al and α-Al_2O_3.

	Exp. (mj/m^2)	EAM	ReaxFF (2004)	ReaxFF (2014)
Al_2O_3 (700 K)	2600 [a] , 2640 [b]	------	444 (mj/m^2)	1830 (mj/m^2)
Al (700 K)	1270 [c]	1044 (mj/m^2)	531 (mj/m^2)	675 (mj/m^2)

[a] Reference [56]
[b] Reference [57]
[c] Reference [58]

4.5. Details of Wetting Simulations

In this section, the computational details of the wetting simulations of aluminum and alumina system using ReaxFF potentials are discussed. The wetting simulations are performed under vacuum –used to note that no vapor phase exists- environment using NVT ensemble with the constant temperature and volume. Selecting eight different temperatures and four different aluminum droplet sizes we aimed at investigating the size and temperature effect. Periodic boundary conditions are imposed in x, y, z directions. However, we allowed a suitable vacuum distance between the boundary in +z direction and the last layer of atoms on the alumina surface, appropriate to place the droplet and avoid periodic boundary conditions to have any influence on the system in z- and as well as in other directions, i.e. periodic boundary conditions will not have any effect on molten aluminum droplets. The length of simulations is 70 ps for each temperature and droplet size. The equilibrium simulations is defined as the time range the contact angle became nearly constant which is nearly 20 to 70 ps – over which the contact angle analysis and chemical analysis of interface regions conducted.

In wetting simulations, we used 4 different size aluminum droplets with the diameters 16, 24, 32, 40 Å. The droplets contain aluminum atoms range from 130 (for 16 Å) to 2000 (for 40 Å). However, the number of atoms in a droplet change as a function of droplet size, temperature effect (thermal expansion), configurations of atoms, and volumetric density difference resulted from potentials such as EAM or ReaxFF. Therefore, each droplet in the wetting simulations has slightly different number of atoms and atom configurations. Yet the number of atoms is quite close to each other at the

same size droplet. Atomic configurations for aluminum droplets are specifically chosen from aluminum cooling simulations to create well equilibrated droplets to be used in the wetting and chemical structure simulations. Note, on cooling cycle simulations it is within the temperature ranges are in molten phase.

Wetting simulations are performed with droplet models in which the aluminum droplet is placed on the alumina substrate. Three different kinds of alumina layers are used in substrate to create realistic wetting simulations. First the alumina layer is relaxed surface layer obtained from the bottom part (slab) of last frame of surface formation energy simulations. Second and third layers are picked up from the last frames of heating simulations for each hundred K temperatures. At first and second layer, atoms are free to move, which means there is no other force than interatomic forces. However, third layer atoms are rigid body, from which the internal force don't count but external forces cause movement as a single body (rigid body).

The droplet model consists of combinations of the aluminum droplet, and three layers of alumina substrate. The three layer of alumina replicated x and y directions without empty space or overlap between aluminum layer to create big enough substrate for wetting simulations. However, 2 Å separation are applied between droplet and alumina layers. Figure 32 shows the Procedures of creating wetting simulations.

Table 9 shows number of atoms for droplet and substrate depend on system size (diameter of droplet) and temperature. The length of simulation boxes for x and y directions are given.

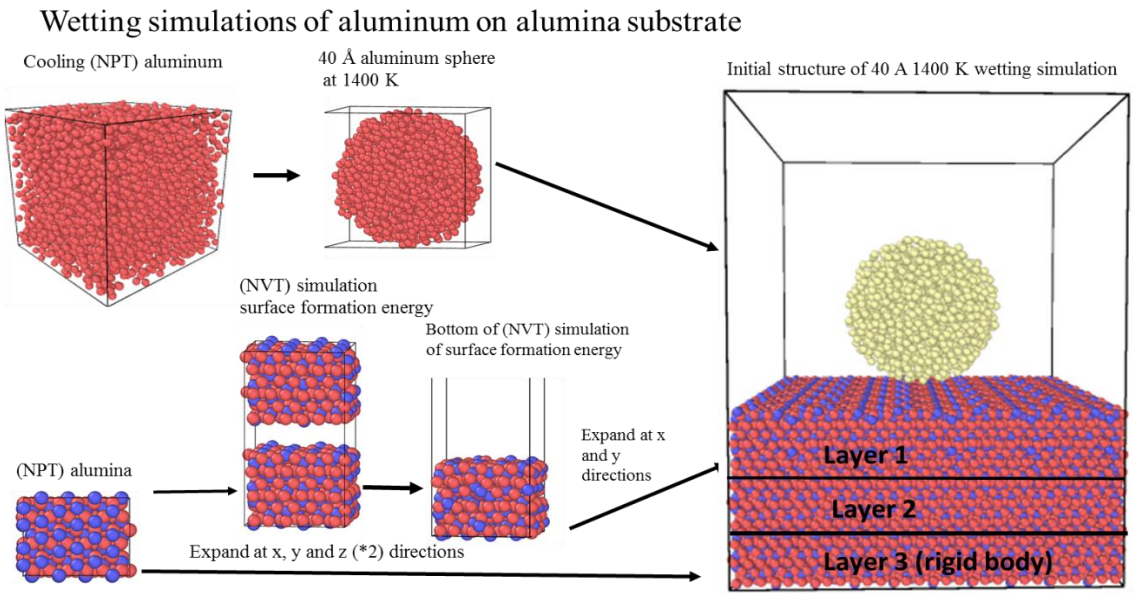

Figure 32: The snapshots, schematically represents the creating process of initial structure of wetting simulations for 40 Å at the 1000 K

Table 9: Number of atoms in sphere and substrate (subs.) respect to temperature and sphere (sph.) diameter 16, 24, 32 and 40 Å. Lx and Ly are the length of simulations box at x and y directions, respectively.

	16 (Å)				24 (Å)			
T (K)	Sph.	Subs.	Lx (Å)	Ly (Å)	Sph.	Subs.	Lx (Å)	Ly (Å)
700	111	4320	33.48	28.99	373	9720	50.22	43.49
800	111	4320	33.53	29.04	366	9720	50.29	43.56
900	103	4320	33.59	29.09	346	9720	50.38	43.63
1000	103	4320	33.63	29.12	337	9720	50.45	43.68
1100	101	4320	33.68	29.16	326	9720	50.52	43.74
1200	89	4320	33.73	29.21	303	9720	50.59	43.81
1300	82	4320	33.77	29.24	291	9720	50.66	43.87
1400	74	4320	33.80	29.29	254	9720	50.71	43.94
	32 (Å)				40 (Å)			
T (K)	Sph.	Subs.	Lx (Å)	Ly (Å)	Sph.	Subs.	Lx (Å)	Ly (Å)
700	868	21600	66.96	72.49	1705	32400	83.70	86.98
800	855	21600	67.06	72.60	1676	32400	83.82	87.13
900	828	21600	67.17	72.72	1592	32400	83.96	87.26
1000	793	21600	67.26	72.81	1545	32400	84.08	87.37
1100	763	21600	67.36	72.90	1479	32400	84.20	87.48
1200	737	21600	67.45	73.02	1424	32400	84.31	87.62
1300	684	21600	67.55	73.11	1342	32400	84.43	87.73
1400	580	21600	67.61	73.24	1178	32400	84.51	87.88

Figure 33 shows the initial structures for 4 different droplet size (16, 24, 32, 40 Å) at the temperature 700 K. The number of atoms in each sphere and substrate size is defined at Table 9. In wetting simulations, each alumina substrate has a 3 alumina z lattice parameter thickness. Therefore, the thickness of substrates is around 39 to 40 Å. Additionally, there is a 2 Å separation between the substrate and sphere. However, sphere diameters and substrate sizes at x and y directions change dramatically. Therefore, the number of atom are different at each wetting simulations.

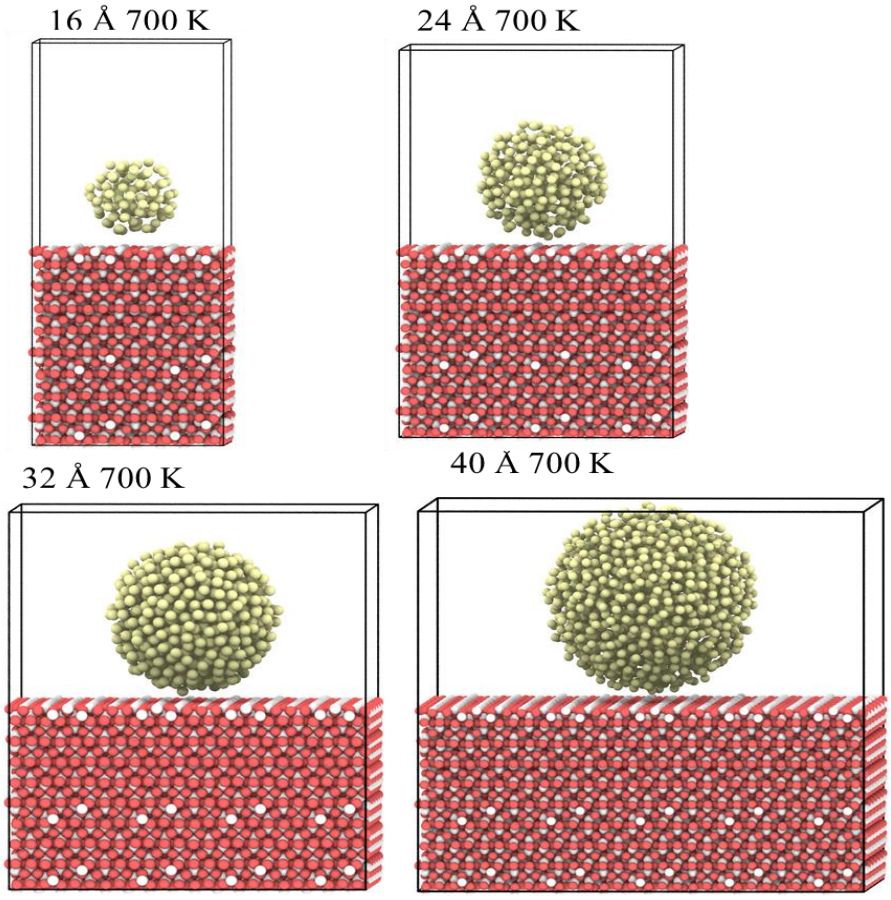

Figure 33: Snapshot of last frame of wetting simulations for four different droplets at the 700 K

4.6. Results of Wetting Simulations

Wetting properties of aluminum droplet on the alumina substrate is studied with four different droplet size and 8 different temperatures from 700 to 1400 K using ReaxFF (2014). Contact angles of these simulations are found by using the method of Hautman and Klein [53]. Additionally, one body density of aluminum and alumina atoms along the z directions is studied. Figure 34 shows the snapshots of wetting simulation of 32 Å and 700 K at different times 0, 5, 10, 20, 40 and 70 ps.

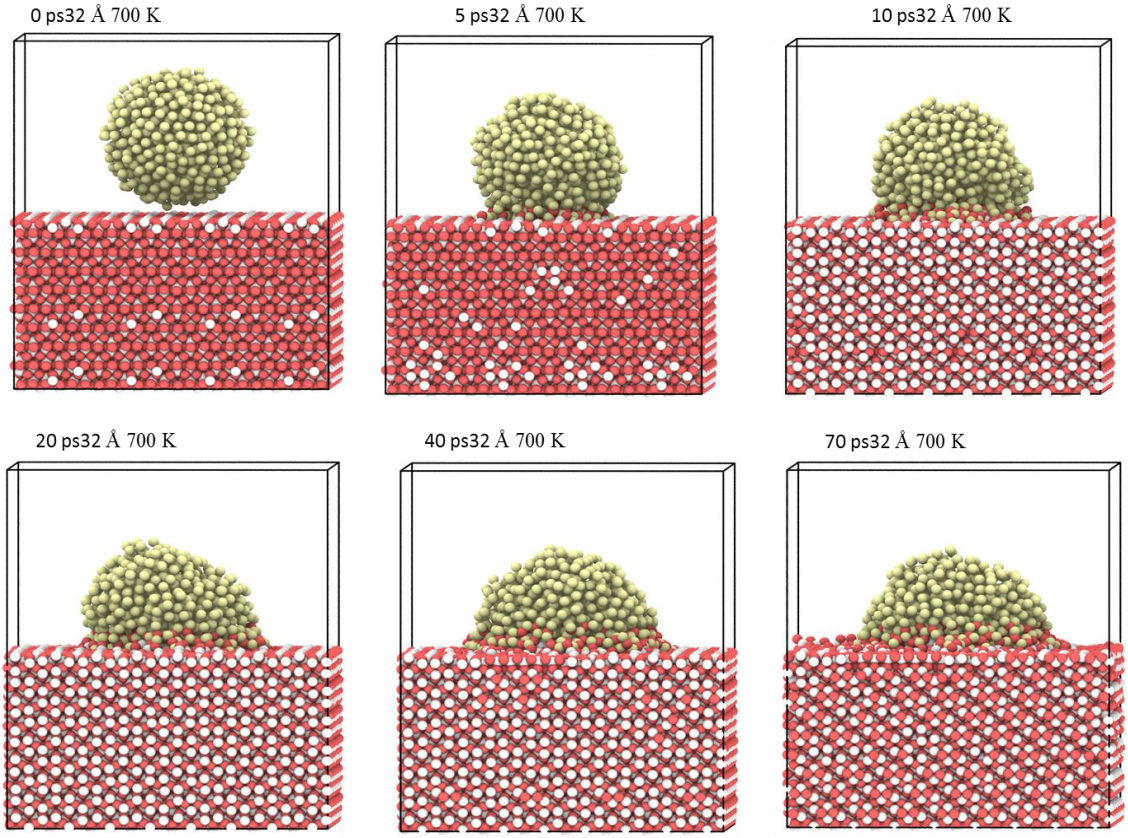

Figure 34: Snapshots of wetting simulations at 40 Å 700 K for 0, 5, 10, 20, 40, 70 ps.

Figure 35 shows the number of oxygen density related distances in the z direction for 40 Å at 1000 K and 0 and 67 ps. At 0 ps, which is represented by black line, there is no oxygen atoms after 40 Å. However, the oxygen number density increases at the z distance from 40 to 50 Å. Consequently, around 35 to 40 Å it is decreased. These results show that some of the oxygen atoms diffuse into the molten aluminum drop within a range of 10 Å.

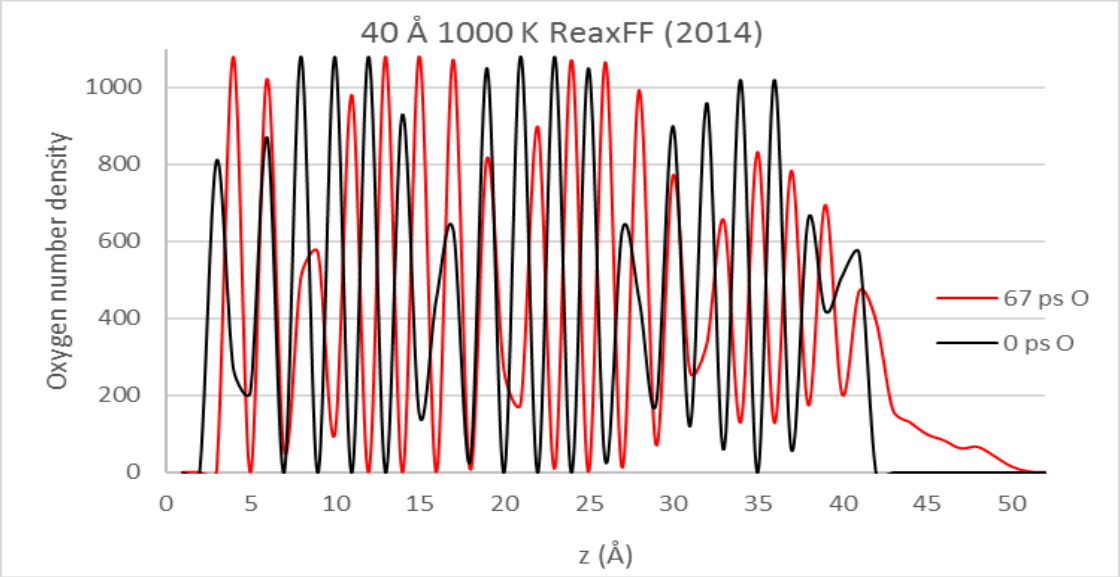

Figure 35: The oxygen number density of wetting simulations at 40 Å at 1000 K for initial (0 ps) and 67 ps.

Figure 36 shows the aluminum density along z direction. The aluminum belongs to the alumina at the initial structures, however even some of the aluminum atoms from the alumina surface move and merge into the liquid droplet aluminum. This can be seen

from the tail of the plot in Figure 36, when one compare g(z) for 0 ps (black line) and 67 ps (red line). At 67 ps simulations aluminum atoms diffused close to 5 Å.

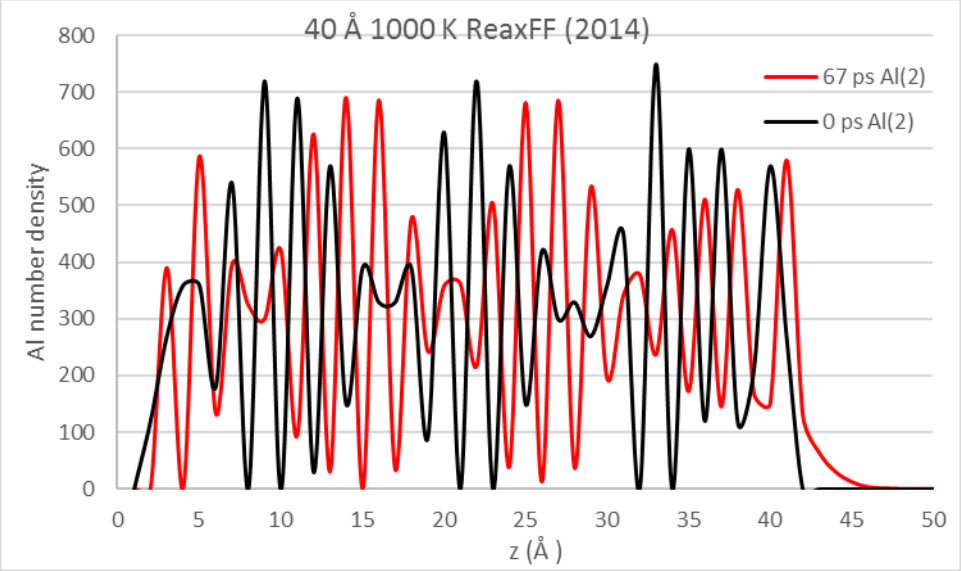

Figure 36: The aluminum (come from alumina) number density of wetting simulations at 40 Å at 1000 K for initial (0 ps) and 67 ps. Al(2) represent the aluminum compound of alumina.

Figure 37 shows the number of density of aluminum atoms of liquid droplet in z directions. 1-body density of molten droplet aluminum along z-direction have an envelope shaped as a semi-circle as expected, i.e. the spherical molten droplet, non-zero probability is between 43 to 83 Å for the 40-Å radius spherical droplet at 0 ps.

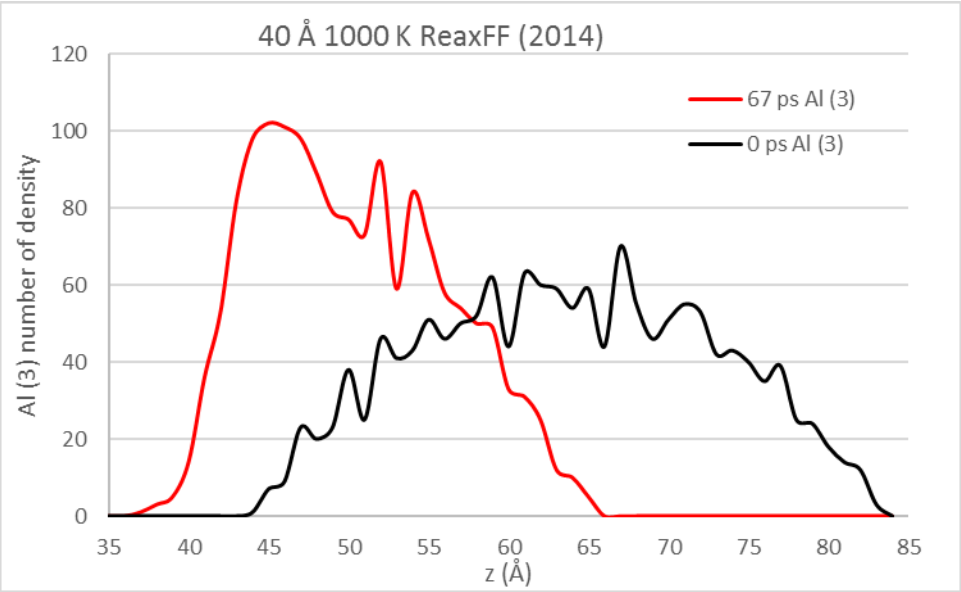

Figure 37: The aluminum (come from droplet) number density of wetting simulations at 40 Å at 1000 K for initial (0 ps) and 67 ps. Al(3) represent the alumina of liquid droplet.

Figure 38 shows one body densities along z-direction for oxygen -from alumina-, for Al (2) from Alumina and for Al (3) from molten aluminum droplet separately. A most significant observation from this analysis at this particular frame (67 ps) is there is a substantial probability density for existence within the droplet; and small interdiffusion of Al (2) and Al (3) into each other domains (metal into metal oxide, though smaller than the metal from molten metal to metal oxide.

In figure 39, we have investigated maximum extension of oxygen from ceramic to molten metal drop, Aluminum from molten metal to ceramic, Aluminum ceramic to aluminum droplet by finding maximum and minimum values of aluminum atoms at z direction for droplet Al (3) and maximum values of aluminum (Al (2)) and oxygen atoms from ceramic (alumina substrate). The largest excursion is about 10 angstrom for

oxygens, maximum extent of motion for Al(2) and Al(3) are around 5 angstroms. 0 at z direction represents the surface (interface) of alumina substrate.

In Figure 40, we show the variation of contact angle as a function of time during simulation of 32 Å droplet at 900 K. Measured contact angles were calculated using the section of the data where both chemical and structural equilibrium is reached (flat behavior in Zcm and associated contact angle). We have listed the equilibrium values of the contact angles in Table 10, for all sizes of droplet and all temperatures where simulations are carried over. One should notice that the droplets of size 16 and 24 Å give rise to a scatter as a function of temperature, due to extent of active interface chemistry for simulations started from perfect crystalline 0001 surface of alumina and molten metal. This active surface chemistry for smaller droplet sizes involves a significant fraction of aluminum atoms from the surface of molten droplet as opposed to larger droplets the surface-active aluminum as less than 10 of the aluminum atoms from the droplets reaches a stable interface structure and enables us to obtain equilibrium wetting configurations. Indeed, the most reliable results for the contact angle measurements are those obtained from the droplets of 40 A. The results indicate that earlier studies conducted by Zhang et al [13] with a fixed alumina slab though provided the contact angle measurements for ReaxFF (2004), but have not included the influence of active interface chemistry.

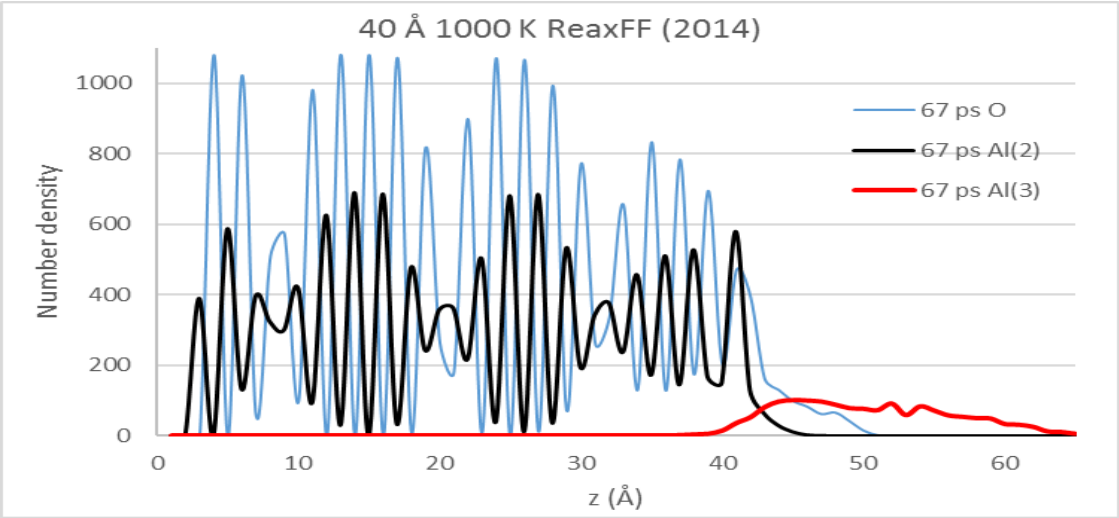

Figure 38: Nnumber densities of oxygen Al (2) and Al (3) of wetting simulations at 40 Å at 1000 K at 67 ps. Al(3) represent the alumina of liquid droplet and Al (2) represent the aluminum come from alumina.

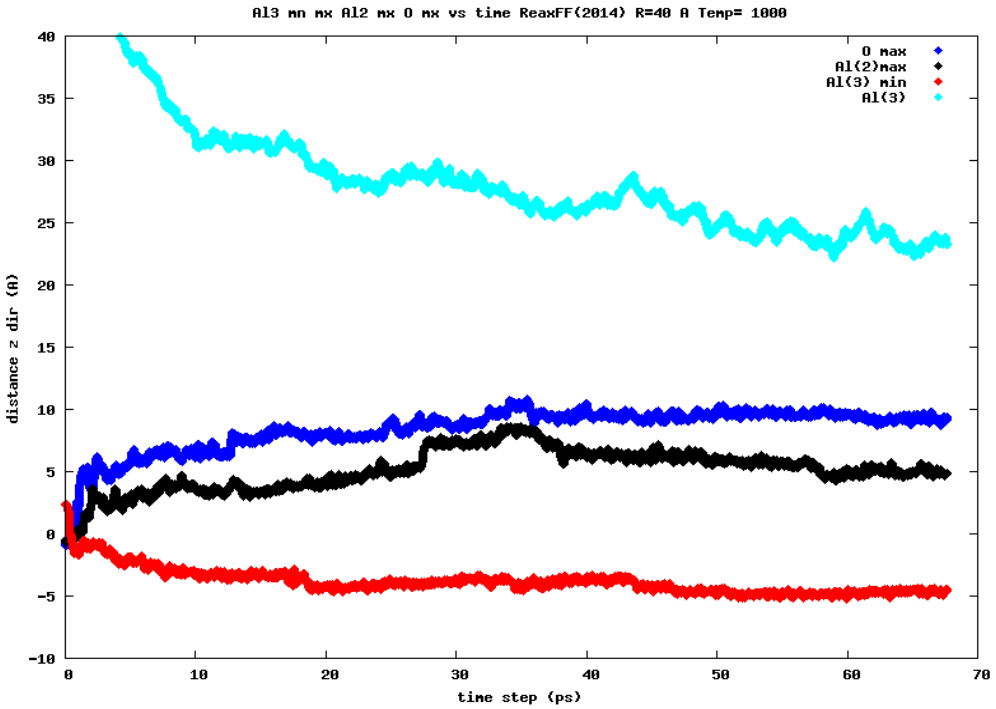

Figure 39: The max range of oxygen, aluminum come from alumina (Al(2)) and Al come from droplet (Al(3)) atoms at z directions. And light blue shows the minimum range of Al (3) at z directions. In the graph, z=0 is the surface of alumina substrata (interface at z directions).

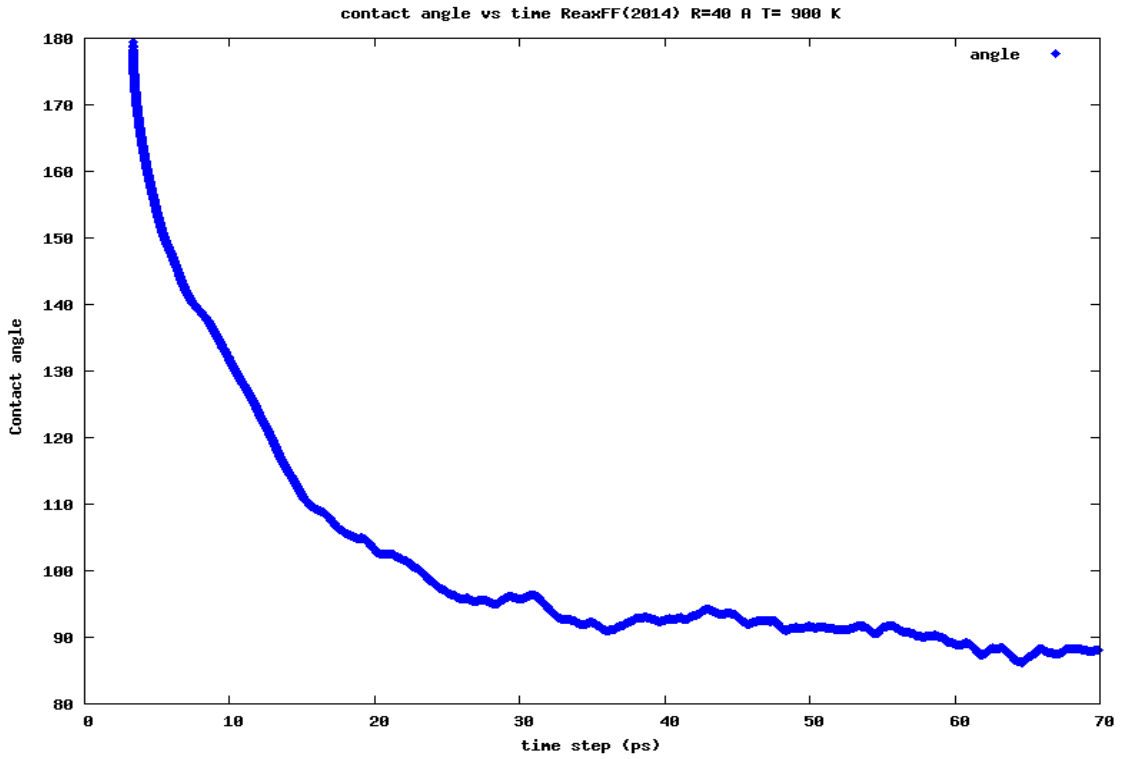

Figure 40: The time (ps) vs contact angle of wetting simulation at 40 Å aluminum droplet and 900 K temperatures. There is sharp decrease until 20 ps, and equilibrium around 89 ˚ from 30 to 70 ps.

Table 10: Contact angle of wetting simulations using ReaxFF (2014) for different temperatures from 700 to 1400 K and different droplet size (the diameter is 16, 24, 32 ,40 Å)

T (K)	16 Å	24 Å	32 Å	40 Å
700	68	77	96	111
800	44	64	83	102
900	46	64	71	89
1000	31	60	80	81
1100	34	49	59	84
1200	34	38	53	55
1300	20	32	49	51
1400	25	41	45	45

The contact angle of aluminum droplet on alumina substrate have tendency decrease with increasing at the temperatures. Additionally, contact angles increase with the droplet size at the same temperatures (shown in Figure 41). For example, contact angles are 68, 77, 96, 111˚, and size of droplet is 16, 24, 32 and 40 Å at the 700 K, respectively.

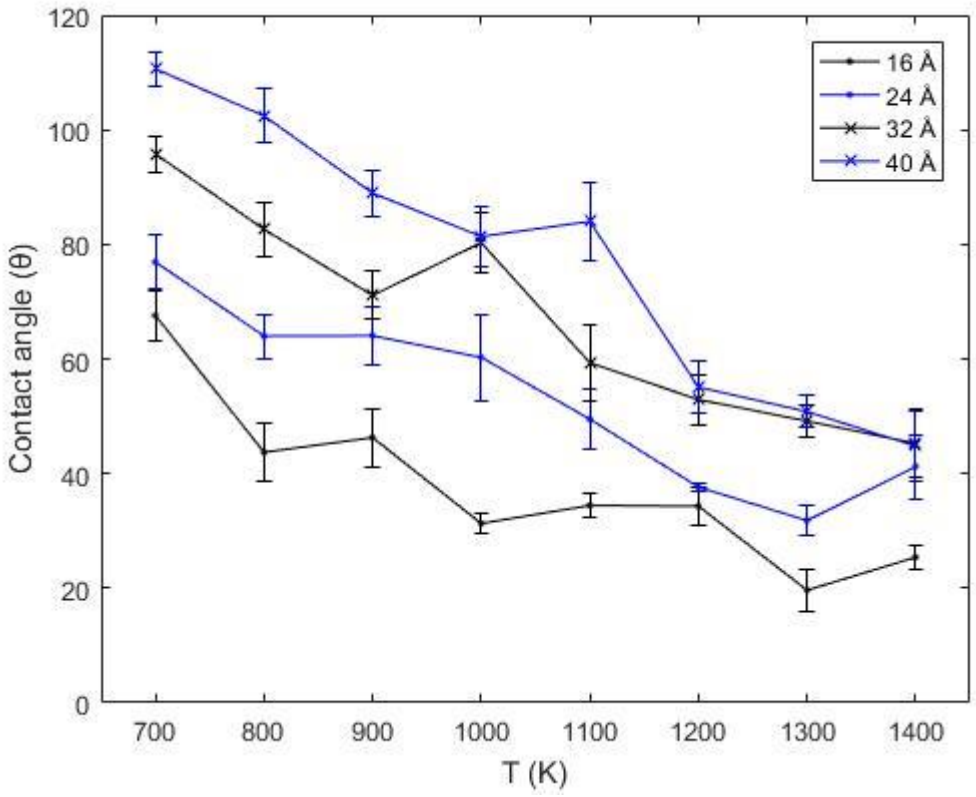

Figure 41: The temperature and contact angle curves of wetting simulations using ReaxFF (2014) for four different droplet size and temperatures from 700 to 1400 K.

5. CONCLUSION REMARKS

In this study, we have investigated thermal, mechanical properties of Al-metal and its oxide, α-alumina using molecular dynamics using state of the art interaction potentials: including two versions of reactive potentials in addition to an EAM potential for Aluminum. The use of reactive potentials is instrumental to address the main objective of this project, the study of interface chemistry for Al/Al_2O_3 interface and wetting of α-Alumina (0001) surface by molten aluminum droplets as a function of temperature and droplet size. We have also studied the surface formation energy of solid-solid Al-Al and Al_2O_3- Al_2O_3 for different temperatures. Temperature and size effect on wetting properties of aluminum droplet on alumina substrate are studied by using ReaxFF potential in particular to see the influence of interface chemistry as opposed to earlier studies.

The thermal and mechanical properties of aluminum and alumina are investigated by using two different potentials which are reactive force field (ReaxFF) and EAM. Thermal properties of Al and Al_2O_3 are studied for different temperatures range from 0 to 1400 K. Mechanical properties are studied for different temperatures ranging from 100 to 900 K with the temperature increment of 200 K. To obtain bulk modulus, mechanical property simulations are performed at different pressures: 0.25, 0.5, 1, 2, 3 and 4 GPa for each isotherm.

The surface formation simulations are also studied different two potential at the temperatures from 700 to 1400 K. The surface formation energies are underestimated by

the three different potentials. However, the result of surface formation energy of EAM is the closest to experimental values for aluminum metal. Additionally, the result of alumina simulation using ReaxFF (2014) is closer to experimental values for alumina than to the ReaxFF (2004). These surface formation energy simulations basically had two main purposes, one of which was to obtain the surface formation energy and the other was to acquire the relaxed alumina surface to utilize in wetting simulations. The results of surface formation energy simulations were used in wetting simulations as the initial structures to be wetted by molten aluminum droplets.

We performed wetting simulations at different temperatures and sizes to obtain the contact angle as a measure of the wettability of aluminum on alumina. The wetting simulation performed by using ReaxFF (2014). In wetting simulations, we found the contact angle for range in temperature from 700 K to 1400 K. Also, we investigated the size effect on wetting simulations. To study the size effect, we have utilized four different diameter droplets which are 16, 24, 32, and 40 Å.

We observe chemical reactions at all temperatures and different droplet sizes, some of the oxygen atoms diffused into the aluminum droplets during wetting simulations. Simultaneously, some of the aluminum atoms from the alumina substrate diffused into the aluminum droplets and the aluminum atoms from the droplets moved into the alumina substrate. During diffusion, some of the Al-Al, Al-O bonds broke and new bonds formed in the aluminum-alumina interface. Therefore, the chemical reactions occur during wetting.

In 16 Å wetting simulation, there are wide scattering at the calculated contact angles. Surface to volume ratio of 16 Å droplets are very high compared to 32 and 40 Å droplets. Therefore, in 16 Å simulations, chemical reactions are more effective than the wetting phenomenon. Nearly all atoms of aluminum droplet form bonds between oxygen atoms and alumina.

The result of 32 and 40 Å wetting simulations are close to experimental values even if there is a small scattering at the result. The scattering caused by chemical reactions between aluminum droplets and alumina substrate during the wetting simulation some of the aluminum atoms diffused into alumina substrate and that affected the result of calculated center of mass of aluminum droplet along z direction. Therefore, contact angle can be lower than reality. To prevent that better approximation to calculate center of mass of droplet should be developed. Another option is to create larger simulations at which surface volume ratio is even lower than 40 Å droplet case which means droplet sizes larger than 40 Å may have to be employed. This, in turn, requires using larger lateral area for alumina slab; hence an increase in substrate size over all. The simulations with reactive potentials are several orders of magnitude faster than quantum mechanics based methods, due to complex form of the energy expressions they are almost two orders of magnitude slower than commonly used non-reactive classical potentials.

REFERENCES

1. Aral, G., Parallel molecular dynamics simulations of dynamics of oxidation and reactive wetting in metal/ceramic systems. 2003, Illinois Institute of Technology.
2. Mazumdar, S., What will drive composites growth in 2015. Composites Manufacturing (online), 2015. http://compositesmanufacturingmagazine.com/2015/01/what-will-drive-composites-growth-in-2015.
3. Gibson, R.F., Principles of composite material mechanics. 2016: CRC press.
4. Garbiec, D., et al., Properties of Al–Al 2 O 3 composites synthesized by spark plasma sintering method. Archives of Civil and Mechanical Engineering, 2015. 15(4): p. 933-939.
5. Zhang, Z., et al., The peculiarity of the metal-ceramic interface. Scientific Reports, 2015. 5: p. 11460.
6. Kok, M., Production and mechanical properties of Al 2 O 3 particle-reinforced 2024 aluminium alloy composites. Journal of Materials Processing Technology, 2005. 161(3): p. 381-387.
7. Mazahery, A., H. Abdizadeh, and H. Baharvandi, Development of high-performance A356/nano-Al 2 O 3 composites. Materials Science and Engineering: A, 2009. 518(1): p. 61-64.

8. Sajjadi, S., H. Ezatpour, and H. Beygi, Microstructure and mechanical properties of Al–Al 2 O 3 micro and nano composites fabricated by stir casting. Materials Science and Engineering: A, 2011. 528(29): p. 8765-8771.

9. Van Duin, A.C., et al., ReaxFF: A reactive force field for hydrocarbons. The Journal of Physical Chemistry A, 2001. 105(41): p. 9396-9409.

10. Ksiazek, M., et al., Wetting and bonding strength in Al/Al 2 O 3 system. Materials Science and Engineering: A, 2002. 324(1): p. 162-167.

11. Klinter, A.J., G. Mendoza-Suarez, and R.A. Drew, Wetting of pure aluminum and selected alloys on polycrystalline alumina and sapphire. Materials Science and Engineering: A, 2008. 495(1): p. 147-152.

12. Bao, S., Filtration of aluminium-experiments, wetting, and modelling. 2011, Norwegian University of Science and Technology,.

13. Zhang, Q., et al., Adhesion and nonwetting-wetting transition in the Al/α−Al2O3 interface. Physical Review B, 2004. 69(4): p. 045423.

14. Sarina, B., et al., Wetting of pure aluminum on graphite, SiC and Al 2 O 3 in aluminum filtration. Transactions of Nonferrous Metals Society of China, 2012. 22(8): p. 1930-1938.

15. Wang, D.-J. and S.-T. Wu, The influence of oxidation on the wettability of aluminum on sapphire. Acta Metallurgica et Materialia, 1994. 42(12): p. 4029-4034.

16. Nicholas, M., The strength of metal/alumina interfaces. Journal of Materials Science, 1968. 3(6): p. 571-576.

17. Sangghaleh, A. and M. Halali, An investigation on the wetting of polycrystalline alumina by aluminum. Journal of Materials Processing Technology, 2008. 197(1): p. 156-160.

18. Shen, P., et al., Wetting of (0001) α-Al 2 O 3 single crystals by molten Al. Scripta Materialia, 2003. 48(6): p. 779-784.

19. Nagy, Š., et al., Pre-review study of the aluminum/alumina master alloy made through pressure infiltration. Materials & Design, 2015. 66: p. 1-6.

20. De Coninck, J. and T. Blake, Wetting and molecular dynamics simulations of simple liquids. Annu. Rev. Mater. Res., 2008. 38: p. 1-22.

21. Gee, R.H., et al., Molecular dynamics investigation of adhesion between TATB surfaces and amorphous fluoropolymers. Macromolecules, 2007. 40(9): p. 3422-3428.

22. Hong, S. and A.C. van Duin, Molecular dynamics simulations of the oxidation of aluminum nanoparticles using the ReaxFF reactive force field. The Journal of Physical Chemistry C, 2015. 119(31): p. 17876-17886.

23. Pilania, G., et al., Revisiting the Al/Al2O3 interface: Coherent interfaces and misfit accommodation. Scientific Reports, 2014. 4: p. 4485

24. Zhang, Q., et al., Atomic simulations of kinetic friction and its velocity dependence at A⁄l Al and α− Al 2 O 3⁄α− Al 2 O 3 interfaces. Physical Review B, 2005. 72(4): p. 045406.

25. McDonald, I., NpT-ensemble Monte Carlo calculations for binary liquid mixtures. Molecular Physics, 1972. 23(1): p. 41-58.

26. Valleau, J.P. and L.K. Cohen, Primitive model electrolytes. I. Grand canonical Monte Carlo computations. The Journal of Chemical Physics, 1980. 72(11): p. 5935-5941.

27. Andersen, H.C., Molecular dynamics simulations at constant pressure and/or temperature. The Journal of Chemical Physics, 1980. 72(4): p. 2384-2393.

28. Parrinello, M. and A. Rahman, Polymorphic transitions in single crystals: A new molecular dynamics method. Journal of Applied Physics, 1981. 52(12): p. 7182-7190.

29. Nosé, S., A unified formulation of the constant temperature molecular dynamics methods. The Journal of Chemical Physics, 1984. 81(1): p. 511-519.

30. Hoover, W.G., Canonical dynamics: Equilibrium phase-space distributions. Physical Review A, 1985. 31(3): p. 1695.

31. Çagin, T. and B.M. Pettitt, Grand molecular dynamics: A method for open systems. Molecular Simulation, 1991. 6(1-3): p. 5-26.

32. Çağin, T. and B.M. Pettitt, Molecular dynamics with a variable number of molecules. Molecular Physics, 1991. 72(1): p. 169-175.

33. Liang, T., et al., Reactive potentials for advanced atomistic simulations. Annual Review of Materials Research, 2013. 43: p. 109-129.

34. Senftle, T.P., et al., The ReaxFF reactive force-field: Development, applications and future directions. npj Computational Materials, 2016. 2: p. 15011.

35. Daw, M.S. and M.I. Baskes, Embedded-atom method: Derivation and application to impurities, surfaces, and other defects in metals. Physical Review B, 1984. 29(12): p. 6443.

36. Mishin, Y., et al., Interatomic potentials for monoatomic metals from experimental data and ab initio calculations. Physical Review B, 1999. 59(5): p. 3393.

37. Aktulga, H.M., et al., Parallel reactive molecular dynamics: Numerical methods and algorithmic techniques. Parallel Computing, 2012. 38(4): p. 245-259.

38. Plimpton, S., Fast parallel algorithms for short-range molecular dynamics. Journal of Computational Physics, 1995. 117(1): p. 1-19.

39. Zhang, Q., et al., Origin of static friction and its relationship to adhesion at the atomic scale. Physical Review B, 2007. 75(14): p. 144114.

40. Callister, W.D. and D.G. Rethwisch, Materials science and engineering: An introduction. Vol. 7. 2007: Wiley New York.

41. Nix, F. and D. MacNair, The thermal expansion of pure metals: Copper, gold, aluminum, nickel, and iron. Physical Review, 1941. 60(8): p. 597.

42. Lee, C.-C., et al., An apparatus for the measurement of internal stress and thermal expansion coefficient of metal oxide films. Review of Scientific Instruments, 2001. 72(4): p. 2128-2133.

43. Bodryakov, V.Y. and A. Bykov, Correlation characteristics of the volumetric thermal expansion coefficient and specific heat of corundum. Glass and Ceramics, 2015. 72(1-2): p. 67-70.

44. Qi, Y., et al., Melting and crystallization in Ni nanoclusters: The mesoscale regime. The Journal of Chemical Physics, 2001. 115(1): p. 385-394.

45. Chase, M.W., NIST-JANAF thermochemical tables for oxygen fluorides. The Journal of Chemical Physics, 1996. 25(2): p. 551-603.

46. Gerlich, D. and E. Fisher, The high temperature elastic moduli of aluminum. Journal of Physics and Chemistry of Solids, 1969. 30(5): p. 1197-1205.

47. Pham, H.H., et al., Finite-temperature elasticity of fcc Al: Atomistic simulations and ultrasonic measurements. Physical Review B, 2011. 84(6): p. 064101.

48. Anderson, O.L., D. Isaak, and H. Oda, High-temperature elastic constant data on minerals relevant to geophysics. Reviews of Geophysics, 1992. 30(1): p. 57-90.

49. Shang, S., Y. Wang, and Z.-K. Liu, First-principles elastic constants of α-and θ-Al2O3. Applied Physics Letters, 2007. 90(10): p. 101909.

50. Law, K.-Y. and H. Zhao, Surface wetting: Characterization, contact angle, and fundamentals. 2015: Springer.

51. Young, T., An essay on the cohesion of fluids. Philosophical Transactions of the Royal Society of London, 1805. 95: p. 65-87.

52. Taherian, F., Molecular perspective of static wetting: Simulation and theory. Technische Universität, Darmstadt, 2013.

53. Hautman, J. and M.L. Klein, Microscopic wetting phenomena. Physical Review Letters, 1991. 67(13): p. 1763.

54. Levi, G. and W.D. Kaplan, Oxygen induced interfacial phenomena during wetting of alumina by liquid aluminium. Acta Materialia, 2002. 50(1): p. 75-88.

55. Fan, C.F. and T. Cağin, Wetting of crystalline polymer surfaces: A molecular dynamics simulation. The Journal of Chemical Physics, 1995. 103(20): p. 9053-9061.

56. Navrotsky, A., Energetics of nanoparticle oxides: Interplay between surface energy and polymorphism†. Geochemical Transactions, 2003. 4(1): p. 1-4.

57. McHale, J., et al., Surface energies and thermodynamic phase stability in nanocrystalline aluminas. Science, 1997. 277(5327): p. 788-791.

58. Skriver, H.L. and N. Rosengaard, Surface energy and work function of elemental metals. Physical Review B, 1992. 46(11): p. 7157.